Annual Report

Hydrospheric Atmospheric Research Center (HyARC)

Nagoya University

2009

Annual Report

Hydrospheric Atmospheric Research Center (HyARC)

2009

NAGOYA UNIVERSITY

Contents

Foreword 2

Staff and Organization 3

Research Programme 6

Progress Reports

Projects 8

Division of Regional – Scale Water Cycle Processes 12

Laboratory of Meteorology 12

Laboratory for Climate System Study 18

Laboratory for Cloud and Precipitation Climatology 22

Division of Global – Scale Water Cycle Variations 24

Laboratory of Satellite Meteorology 24

Laboratory of Eco-Hydrometeorology 26

Laboratory of Satellite Biological Oceanography 28

Laboratory of Bio-Physical Oceanography 32

List of Publications 34

Foreword

The Hydrospheric Atmospheric Research Center (HyARC) at Nagoya University was established nine years ago to promote research on the global water cycle, one of the primary components of the Earth system. Research on the global water cycle requires strong and extensive collaboration among science and application communities, and hence HyARC functions as an inter-university collaborative system, in many ways unique in the world.

HyARC has initiated numerous projects and activities. Prominent among these is the International Project Office of the Global Energy and Water Cycle Experiment (GEWEX) Asian Monsoon Experiment (GAME), led by Prof. T. Yasunari, and its various follow-on projects. Additional work has been supported by the following: Grants-in-Aid for Scientific Research; Core Research for Evolutional Science and Technology (CREST) of the Japan Science and Technology Corporation (JST); Global Environment Research Fund; Innovative Program of Climate Change Projection for the 21st Century; and more. In addition, funding from the Ministry of Education, Culture, Sports, Science and Technology, Japan, supported construction of a multiparameter radar system to study water circulation, and funding from the Inter-University Project supported a virtual laboratory for study of the earth's climate diagnostics.

HyARC has also collaborated with numerous institutions, such as the Research Institute of Humanity and Nature (RIHN) and the National Institute of Information and Communication Technology (NICT). As partial contribution to the UNESCO International Hydrology Programme (IHP), HyARC has conducted training courses, funded by the Japan Trust; this year's course was on satellite remote sensing of atmospheric constituents.

In selecting projects and activities, HyARC considers project feasibility, significance, and collaboration requirements. We currently fund 3 research projects and 4 workshops. Although HyARC's permanent staff numbers only 11 (4 professors, 4 associate professors, and 3 assistant professors), we also support many postdoctoral candidates in active research. In addition, we have accepted graduate students in the Department of Environmental Studies.

Nagoya University has adopted a flexible management system that emphasizes accountability yet encourages research publications and outreach programs. Accordingly, and spurred by comments from an outside evaluation committee, we herewith propose to establish a large-scale national/international facility, and a new organization to address its social requirements.

Uyeda Hiroshi
Director
Hydrospheric Atmospheric Research Center

Staff and Organization

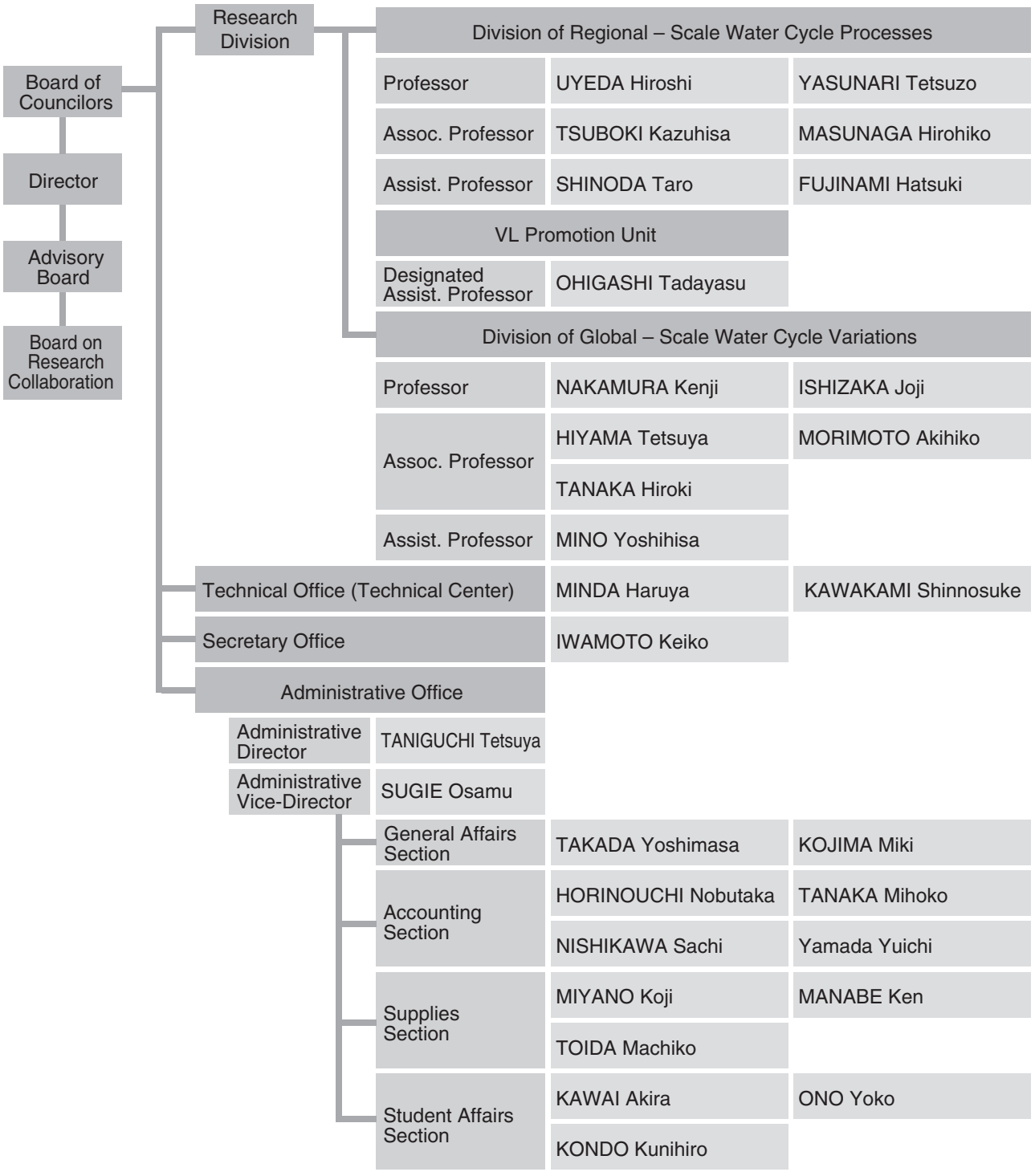

Administration

Board of Councilors

UYEDA Hiroshi: *Director, Prof., Hydrospheric Atmospheric Research Center*

YASUNARI Tetsuzo: *Prof., Hydrospheric Atmospheric Research Center*

NAKAMURA Kenji: *Prof., Hydrospheric Atmospheric Research Center*

ISHIZAKA Joji: *Prof., Hydrospheric Atmospheric Research Center*

TANAKA Kentaro: *Prof., Graduate School of Science*

TSUJIMOTO Tetsuro: *Prof., Graduate School of Engineering*

OTA Takeshi: *Prof., Graduate School of Bioagricultural Sciences*

KANZAWA Hiroshi: *Prof., Graduate School of Environmental Studies*

MATSUMI Yutaka: *Prof., Solar-Terrestrial Environment Laboratory*

Advisory Board

● **Members from Nagoya Unisversity**

YASUNARI Tetsuzo: *Prof., Hydrospheric Atmospheric Research Center*

NAKAMURA Kenji: *Prof., Hydrospheric Atmospheric Research Center*

ISHIZAKA Joji: *Prof., Hydrospheric Atmospheric Research Center*

TSUBOKI Kazuhisa: *Assoc. Prof., Hydrospheric Atmospheric Research Center*

MASUNAGA Hirohiko: *Assoc. Prof., Hydrospheric Atmospheric Research Center*

HIYAMA Tetsuya: *Assoc. Prof., Hydrospheric Atmospheric Research Center*

MORIMOTO Akihiko: *Assoc. Prof., Hydrospheric Atmospheric Research Center*

● **Members outside Nagoya University**

FUJIYOSHI Yasushi: *Prof., Institute of Low Temperature Science, Hokkaido University*

HANAWA Kimio: *Prof., Graduate School of Science, Tohoku University*

SUMI Akimasa: *Prof., Integrated Research System for Sustainability Science, The University of Tokyo*

FUKUSHIMA Yoshihiro: *Prof., Tottori University of Environmental Studies*

YAMANAKA Manabu: *Senior Scientist, Institute of Observational Research for Global Change,Japan Agency for Marine-Earth Science and Technology*

YAMANOUCHI Takashi: *Prof., National Institute of Polar Research*

TANIGUCHI Makoto: *Prof., Research Institute for Humanity and Nature*

OKI Riko: *Senior Researcher, Earth Observation Research Center, Japan Aerospace Exploration Agency*

Board on Research Collaboration

● **Members from Nagoya University**

NAKAMURA Kenji: *Prof., Hydrospheric Atmospheric Research Center*

ISHIZAKA Joji: *Prof., Hydrospheric Atmospheric Research Center*

HIYAMA Tetsuya: *Assoc. Prof., Hydrospheric Atmospheric Research Center*

● **Members outside Nagoya University**

FUJIYOSHI Yasushi: *Prof., Institute of Low Temperature Science, Hokkaido University*

YAMANAKA Manabu: *Senior Scientist, Institute of Observational Research for Global Change, Japan Agency for Marine-Earth Science and Technology*

TANIGUCHI Makoto: *Prof., Research Institute for Humanity and Nature*

OKI Riko: *Senior Researcher, Earth Observation Research Center, Japan Aerospace Exploration Agency*

Research Programme

Water circulation studies using new polarimetric radar

A new polarimetric (multi-parameter) radar was installed at the Hydrospheric Atmospheric Research Center (HyARC), Nagoya University, in 2007. Since installation, this equipment has been promoting new studies on clouds and precipitation, and aiding in the development of new observational and analytical techniques that are essential for studies on water circulation. Such observational and analytical techniques, as well as data assimilation methods, are necessary for the utilization of observational data from the new radar and for amalgamation of the data with a cloud-resolving model.

This research plan aims at promoting new research on water circulation using the new polarimetric radar as well as existing radar sets. In concrete terms, we examine and implement observational data of weather phenomena and physical processes of cloud and precipitation systems. We aim at developing new parameters for multi-parameter radar observation and data analysis and new display methods for radar data. We will develop software and operational routines for the radar from physical and engineering viewpoints in collaboration with researchers participating in this study project.

Diurnal processes of convection/precipitation systems in the climate System

Diurnal variation in convection and precipitation is a prominent meteorological feature, particularly in the tropics/subtropics and monsoon regions. Energy, water, and momentum exchanges through the diurnal cycle between the earth surface, atmospheric boundary layer, and free atmosphere play a crucial role in global climate models (GCMs) and still cannot reproduce a realistic diurnal cycle in convection/precipitation, including systematic errors in the models.

This research plan aims to clarify the regionality and seasonality of diurnal processes based on TRMM, other remote sensing data, and *in-situ* observational data from rain gauge stations. Cloud resolving models (e.g., CReSS and WRF) and other regional models are also used to elucidate systematic errors in the climate model due to the diurnal cycle. These studies can contribute to the ongoing international project "MAHASRI." We aim to promote studies on the diurnal process of convection/precipitation in the climate system in Japan.

On December 19, 2007, a domestic workshop, co-hosted by MAHASRI, was held in Hakone. Studies on the diurnal variation of cloud/precipitation systems, including the relationship with terrain, synoptic conditions and intraseasonal variation, were presented. These studies covered areas from the Tibetan Plateau to the Maritime continents. In total, 14 participants presented new scientific results and there was a lively discussion with many participants in the workshop. Future issues on diurnal cycles were also discussed.

Study of atmospheric and oceanic climate over Okinawa Islands and its surroundings

The National Institute of Information and Communication Technology (NICT) established an observation facility in Okinawa, Japan (Okinawa Subtropical Environment Remote Sensing Center). The facilities provided include a full polarimetric Doppler radar (COBRA), 400-MHz wind profiler radar, Doppler sodar, disdrometers, rain gauges, and ocean radars. In 2005, an interuniversity collaboration between NICT Okinawa and the Hydrospheric Atmospheric Research Center at Nagoya University, Japan (HyARC) started.

The spatial and temporal variations in the Kuroshio Current around the Okinawa Islands were studied using an ocean radar and raindrop-size-distribution characteristics were determined by COBRA polarimetric data. The studies on ocean currents and precipitation are separate; however, if merged, the ocean–atmosphere interaction can be studied. New techniques were developed to study the atmosphere and the oceans (e.g., a flexible ocean radar and a new acoustic speaker system for the radio acoustic sounding system (RASS). Calibration techniques of satellite measurements were also investigated.

NICT is an agency for sensor development using radiowaves, and HyARC organizes the users for exploring deeper and wider applications. Here, the collaboration was well coordinated, and many interesting results were obtained. However, for studying the climate, full utilization of the recorded data is not yet attained. Based on the deep understanding of sensors, a thorough analysis of the data should be conducted.

PROGRESS REPORTS

8

PROJECTS

Formation of a virtual laboratory for diagnosing the earth's climate system

Two polarimetric radars installed in November 2007 started full-scale operation in 2009, after about a year of preparation. In this report, HyARC VL (Virtual Laboratory) Office's efforts in the operation and study of the polarimetric radars in 2009 are summarized.

Long-term observations at Nobi Plain were conducted in 2009. The main radar system, which is called KIN radar, was installed on top of the HyARC building, and has worked efficiently throughout the year without encountering any serious problems. The sub-radar system, which is called GIN radar, was operated at Gifu University from April 2009 to July 2009, and at Anjo Branch, Toyohashi Office of River Works, Ministry of Land, Infrastructure, Transport and Tourism (MLIT), from August 2009 to January 2010. In October 2009, Typhoon 0918 passed through the radar observation areas. Two radars at HyARC and Anjo sites successfully observed strong winds and intense rainfalls at around the typhoon's landfall.

At the Anjo site, an operational X-band polarimetric radar of MLIT has started observation since February 2010. HyARC radar observations at the same location were considered as preliminary observations. We contributed to the study of the observational modes of operational radars at MLIT using HyARC radar's data at the Anjo site.

To enable prompt and adequate response in case a glitch is experienced in the radar systems during the observations, we installed web cameras to remotely monitor radar conditions in association with the HyARC Technical Office.

We created analysis programs to derive polarimetric parameters and study the structure of precipitation systems. We also discussed the Japanese names of the polarimetric parameters, because they have not yet been unified under a common language discussions of the names can be found on the Japanese website (http://www.rain.hyarc.nagoya-u.ac.jp/MPradar/meetings/20090116.html). Some of the names we proposed after the discussion have been adopted in the book written by Professor Fukao and Dr Hamazu in 2009 (ISBN: 9784876987887). In addition, a report on the outline of HyARC radars and the operation from 2007 to 2009 has been compiled for a planned study of HyARC in 2009.

The release of the polarimetric radar data is under preparation. All observational data from April 2009 has been archived. We considered data policy and data format to release the data after 2010.

The Innovative Program of Climate Change Projection for the 21st Century (KAKUSHIN Program)

● Cloud Modeling and Typhoon Research

Cloud physics is a key process for modeling climate changes, especially for global warming. The improvement of cloud processes is necessary for accurate simulations. Cloud processes are also core processes in simulations of high-impact weather systems such as heavy rainfalls and typhoons. The cloud modeling team has been developing a cloud-resolving model named the Cloud Resolving Storm Simulator (CReSS). The cloud microphysics and computation scheme of CReSS are improved for accurate and high-speed calculations. Convective clouds in tropical regions and typhoons are important to our team. The CReSS model is also coupled with global models to simulate convective regions. CReSS is used for typhoon research that aims at verifying typhoon simulations performed by global models and producing accurate and quantitative evaluations of typhoon effects on human society under the current and warming climates.

Typhoons occasionally cause a severe disaster owing to heavy rainfall and strong wind. On the other hand, they bring a large amount of water resources to the East Asian countries. Thus, typhoon changes with global warming have a large impact on the human society. Since typhoons are composed of intense convective clouds as well as associated stratiform clouds, a cloud-resolving simulation is necessary for accurate prediction of their intensities. In the present study, we have developed a new technique to perform a parallel computation of the cloud-resolving model in an arbitrary-shaped region, which is named as the "Tiling Domain Technique" for CReSS. Using this technique, a simulation experiment with a computational domain along the typhoon track was performed. The figure compares the simulation result at 312 h from the initial time (09 JST August 25, 2004) with the radar observation provided by the Japan Meteorological Agency (JMA). The position of the typhoon center, eye wall, surrounding spiral rainband, and orographically enhanced heavy rainfall are correctly simulated. The simulation shows the sea level pressure at the typhoon center also corresponds to the observation. The result shows that the cloud-resolving simulation enables us to predict quantitatively the intensity of a typhoon. In collaboration with the other team of the KAKUSHIN program, our team performed simulation experiments of typhoon under global warming and found that very intense typhoons, which never occurred in the current climate, might occur in future climate.

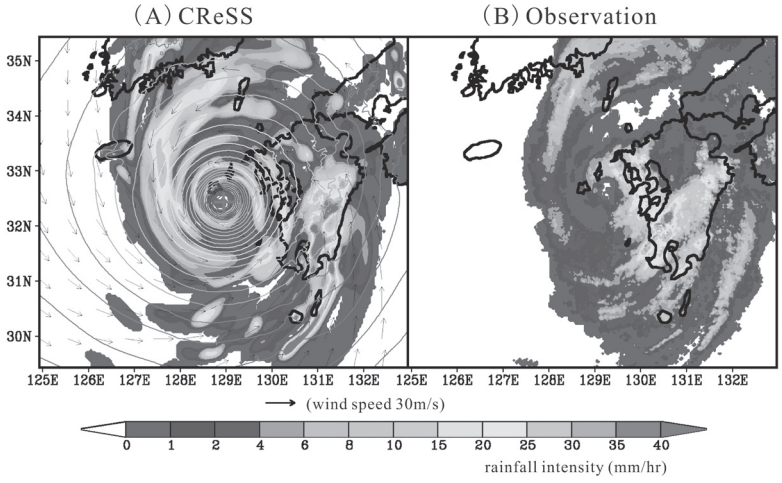

Figure (A) Simulation result of typhoon No.18 of 2004 using CReSS with the Tiling Domain Technique at 312 h from the initial time (09 JST August 25, 2004). Color levels represent rainfall intensity (mm hr^{-1}), contours represent sea level pressure, and arrows represent horizontal velocity. (B) JMA radar observation at the same time of (A). Color levels represent rainfall intensity (mm hr^{-1}).

Solution-Oriented Research in Science and Technology (SORST)

• Satellite Monitoring of Ocean Primary Productivity

The ocean is the largest reservoir of water and carbon dioxide on Earth's surface. Hence, the air-sea exchange of water and carbon dioxide plays a central role in climate systems on Earth. The air-sea exchange of heat (water) and carbon dioxide is affected by phytoplankton because they determine the optical properties of the near-surface oceans and absorb carbon dioxide by primary productivity. To predict climate variability accurately, quantitative knowledge of the abundance and productivity of phytoplankton on a global scale is required for mechanistic understanding of their regulatory processes. In practice, this knowledge and understanding can be attained only by satellite observations, but because of difficulty in obtaining in situ data for validation, available satellite data are yet to be fully exploited.

To overcome this difficulty, we have been working to develop an in situ monitoring system for validation of ocean primary productivity data from satellites. The system, composed of an underwater winch system having a profiler buoy equipped with a fast-repetition-rate fluorometer, was successfully developed with the support of Core Research for Evolutional Science and Technology (CREST) by the Japan Science and Technology Agency (JST). Following this, a continuation project, Satellite Monitoring of Ocean Primary Productivity (SMOPP), was approved by the JST as part of the Solution-Oriented Research in Science and Technology (SORST) Program in 2004. The objective of the SMOPP project is to design an operational monitoring system for ocean primary productivity on a global scale. For this purpose, we conducted routine operation of the monitoring system and obtained validated time series satellite data on primary productivity. These data were used, in combination with other time series satellite data on physical forcing parameters of the ocean's surface, for process studies on the response of ocean biology to atmospheric forcing.

FY2009 was the last year of this CREST/SORST project, and the results were discussed twice, in our internal workshops in October and December. We hosted the International Symposium on Estimation of Ocean/Land Primary Production by Satellite in collaboration with another SORST project (at Chiba University), to apply our results to the Global Change Observation Mission-Carbon (GCOM-C) of the Japan Aerospace Exploration Agency (JAXA).

A notable achievement of this project is that we have developed and established an in situ monitoring system for ocean productivity (the POPPS buoy system), which was corroborated by successful operations in both nearshore and offshore (deep water) areas. The operation in Sagami Bay during 2007–2008 provided the first-ever long-term (year-long) continuous measurements of daily ocean productivity, demonstrating the utility of our system. The POPPS buoy system was adopted as the main instrument for stationary observations in the western subtropical/subarctic North Pacific, conducted under the five-year (2009–2013) research program of the Japan Agency for Marine-Earth Science and Technology (JAMSTEC). Further development of this system in various regions would advance validation for satellite-based productivity, and the consequent use of the validated time series satellite data would enable a breakthrough in the study of ocean material cycling and its response to climate change. As other deliverables, we built an online database containing our research results during this project; it includes enormous numbers of measurements from hydrographic observations in Sagami Bay/Tokyo Bay as well as from POPPS buoy deployments. Measurements are also included from our custom-made Primary Productivity Profiler in various environments (the northern North Pacific, East China Sea, Sea of Japan, and Arabian Sea). These data will contribute to further understanding of the natural variability of oceanic productivity.

Study consortium for Earth-Life Interactive System (SELIS)

The Study consortiumu for Earth-Life Interactive System (SELIS) was established as a virtual institute in Nagoya University in March 2008, to follow up the research activity of the 21st century COE Program of "the Sun-Earth-Life Interactive System". The member instate of SELIS are HyARC, Graduate School of Environmental Sciences (GSES), Graduate School of Bio-Agricultural Sciences (GSBS) and the Solar-Terrestrial Environmental Laboratory. The SELIS project office is located at the 5th floor of the Institute for Advanced Research Hall of this campus, and the HyARC is managing this office as a main institute of SELIS. The main objective of the SELIS is to promote coopearative studies and relevant capacity building for the Earth-Life Interaction studies, and to promote collaboration with relevant national and international programs and projects. SELIS is also expected to contribute to research projects proposed from Nagoya University to the Research Institute for Humanity and Nature (RIHN) in Kyoto. In the education program, SELIS contributes to some lecture course and seminars, e.g., "Chikyu-gaku" (Study for the Earth) at the GSES.

In academic year 2009, SELIS organized six interdisciplinary seminars. SELIS also contributes to basic environmental studies and education under the Global COE Program "From Earth System Science to Basic and Clinical Environmental Studies (BCES)" that started in July 2009. The leader of GCOE-BCES Program is Prof. Tetsuzo Yasunari of HyARC. Prof. Hisashi Sato of GCOE took over as the directorship of the SELIS office from Prof. Tetsuya Hiyama of HyARC.

Laboratory of Meteorology

Development of a hydrometeor classification method for X-band polarimetric radars

Polarimetric radars can obtain microphysical information of hydrometeors, such as shape and canting angle, which can be used for hydrometeor classification, using horizontally and vertically polarized waves. Several studies on hydrometeor classification were conducted to understand severe weather mechanisms using S- or C-band polarimetric radar in Northern America and Europe. Polarimetric radars were recently introduced in Japan, and two X-band polarimetric radar systems were introduced at Nagoya University in 2007. This study presents the development of a hydrometeor classification method for X-band polarimetric radars.
The hydrometeor classification method is based on the method for S-band radars in a previous study that uses polarimetric parameters of radar reflectivity (Z_h), differential reflectivity (Z_{dr}), specific differential phase (K_{dp}), correlation coefficient between horizontal and vertical polarization signals (ρ_{hv}), and temperature. This method classifies hydrometeors into 10 categories, including rain, snowflakes, and graupel. It evaluates the probability of each type of hydrometeor with membership functions of polarimetric parameters and temperature with fuzzy logic, and determines the dominant hydrometeor type by its highest probability.

Since K_{dp} depends on wavelength, the membership functions of K_{dp} are modified to X-band radars. The membership functions of temperature including the dependency of relative humidity apply to melting snowflakes. The vertical profiles of temperature and relative humidity are used from ground-based and upper-air sounding observations.

We attempted to apply the classification method to a snowfall event near Nagoya City, a graupel-falling event over Ishikawa Prefecture during winter, and a thunderstorm near Nagoya City during summer. We classified snowflakes using the method corresponding to ground-based particle observation in the snowfall event near Nagoya City. Thus, the classification method worked successfully. In the graupel-falling event, graupel was classified near the area where the Z_h value was high. A well-known vertical hydrometeor distribution in cumulonimbus clouds was classified in the thunderstorm event near Nagoya City (Fig. 1): rain occurs in the lower level; graupel is found near the melting level; and snowflakes and ice crystals are found above the graupel. As we confirmed the existence of graupel, we compared the time series of lightning frequency with that of volume of the graupel region. The lightning strikes began when the volume of graupel was the largest and continued until the graupel region disappeared. This result is consistent with previous studies on lightning strikes.

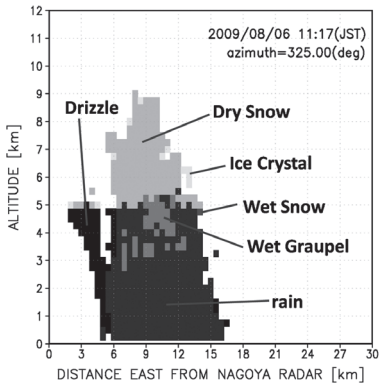

Fig. 1 Result of hydrometeor classification applied to the RHI scan at 1117 JST on August 6, 2009, along the direction of the thunderstorm near Nagoya City. The horizontal axis indicates the distance from the polarimetric radar at Nagoya University.

Raindrop size distribution parameters estimated from polarimetric radar variables in convective cells near Okinawa Island during Baiu period

Convective cells, whose echo-top height reaches around the melting level and develop in a stratiform zone in mesoscale convective systems (MCSs), are observed in humid environment near Okinawa Island during Baiu period. To quantitatively clarify the microphysical characteristics of convective cesslls developing in humid environment, we estimated raindrop size distribution (DSD) parameters in convective cells using parameters such as radar reflectivity (Z_h) and differential reflectivity (Z_{DR}) obtained by the C-band polarimetric radar in Okinawa Island during Baiu period. The DSD parameters are estimated for three types of convective cells: one developing in the stratiform zone, one developing in the convective zone, and an isolated convective cell.

To estimate DSD parameters, their relationship with polarimetric radar variables are used in this study. The median volume diameter (D_0) is estimated by the D_0-Z_{DR} relationship given by Bringi et al. (2006) as follows:

$$D_0 = 4.27\xi_{dr} - 3.71; \quad \text{mm} \quad \text{for } \xi_{dr} < 1.3 \qquad (1)$$

$$D_0 = 0.733\xi_{dr} - 0.909; \quad \text{mm} \quad \text{for } \xi_{dr} > 1.3, \qquad (2)$$

where, $Z_{DR} = 10\log_{10}\xi_{dr}$.

Figure 2a shows the scatter plot between D_0 and ξ_{dr} derived from ground-based DSDs with Eqs. (1) and (2). Although the number of samples for $\xi_{dr} > 1.3$ is not enough in this case, the D_0-Z_{DR} relationship corresponds to the ground-based observation for $\xi_{dr} < 1.3$. The normalized intercept parameter (N_w) that is related to the number concentration of raindrops is estimated using Z_h and D_0 for greater than 3 mm h^{-1} in rainfall rate as follows (Fig. 1b):

$$\frac{N_w}{Z_h} = 4.1\times10^{-2} D_0^{6.93}; \quad \text{mm}^7. \qquad (3)$$

Figure 3 shows the relationships of D_0 and N_w with Z_h obtained in three types of convective cells. For the convective cell in the stratiform zone in the mature stage, the estimated mean D_0 is approximately 1.2 mm with Z_h of 40–45 dBZ; the estimated mean $\log_{10}N_w$ ranges from 32,000 to 100,000 mm^{-1} m^{-3}. For the convective cell in the convective zone in the mature stage, the estimated mean D_0 is approximately 2 mm with Z_h of 40–45 dBZ; the estimated mean $\log_{10}N_w$ range is 1,000–10,000 mm^{-1} m^{-3}. For the isolated convective cell in the mature stage, D_0 is also approximately 2 mm with Z_h of 40–45 dBZ; the estimated mean $\log_{10}N_w$ range is also 1,000–10,000 mm^{-1} m^{-3}. This indicates that a high number concentration of small raindrops contributes to large Z_h for the convective cell in the stratiform zone, whereas a low number concentration of large raindrops contributes to large Z_h for that in the convective zone and isolated cell. The characteristics of the estimated D_0 and N_w for three types of convective cells in the mature stage using the polarimetric radar are also applied for those in other stages.

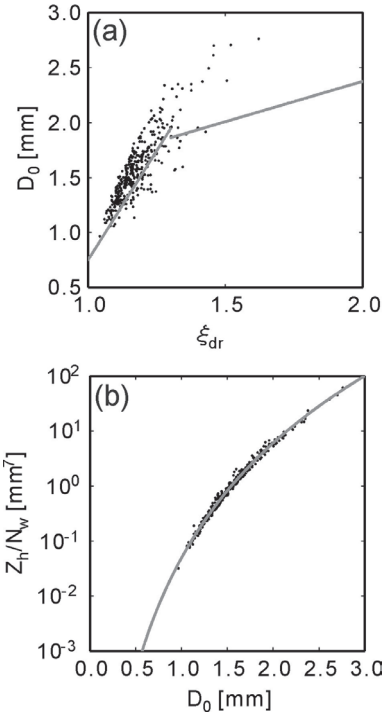

Fig. 2 Scatter plots (dots) and relations (solid lines) for (a) D_0 versus ξ_{dr} and (b) "Z_h/N_w" versus D_0 derived from ground-based DSDs (1 min. integration) with rainfall rate greater than 3 mm h^{-1}. The D_0-ξ_{dr} relation shown by a solid line in (a) is given by Bringi et al. (2006).

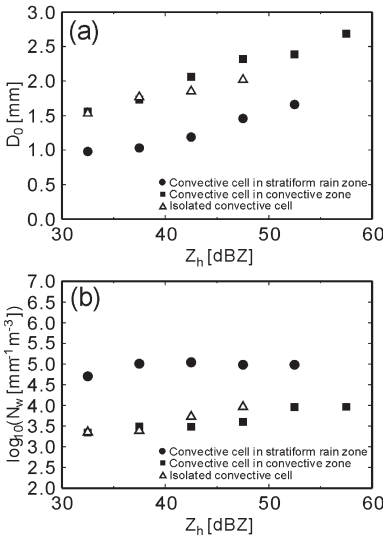

Fig. 3 (a) Relationship between radar-estimated mean D_0 and Z_h for every 5 dBZ and (b) relationship between radar-estimated mean $\log_{10}N_w$ and Z_h for every 5 dBZ for convective cells in their mature stages. The relationships are indicated as (●) for the stratiform zone, (■) for the convective zone, and (△) for the isolated convective cell. The mean values were calculated from the plan position indicator (PPI) data obtained between 0.5 km and 3.0 km above sea level for each convective cell.

Polarimetric radar observation of snow clouds in Hokuriku

In winter season, cold air outbreaks occur from the Eurasian continent in association with the evolution and passage of cyclones. Snow clouds with strong updrafts cover the Sea of Japan; organized snow clouds form convective systems, which cause heavy snowfall and high winds. Many studies have been conducted to clarify their structure and generation/evolution mechanisms. Previous Doppler radar observations examined the airflow structures in clouds. However, there are few studies associated with the distribution and evolution of precipitation particles in snow clouds. A polarimetric radar enables us to obtain information such as shape, size, number density, and attitude of precipitation particles. In order to clarify distribution and evolution of precipitation particles in snow clouds, we performed polarimetric radar observation from December 2008 to February 2009 at Oshimizu of Ishikawa Prefecture in Hokuriku, Japan.

During the observation period, strong cold air outbreaks occurred five times. The radar was operated almost continuously during these events. From January 25 to 27, 2009, a stationary snowband formed along the San-in-Hokuriku coast that caused intense snowfall with frequent lightning. We analyzed polarimetric parameters to show the characteristics of precipitation particles during this event. Radar reflectivity (Z_h) reached 35–40 dBZ near the landing portion (Fig. 4), which suggests frequent intensifications of snow clouds. The frequency of polarimetric parameters is examined in a 10-km square area (white square in Fig. 4) in which the two-day average Z_h was the greatest in the entire radar range. The following frequencies are calculated using the polar-coordinate data obtained by PPI scans. Correlation coefficient (ρ_{hv}) is more than 0.97 at 99% grids; thus, no wet solid particles, such as wet snow and wet graupel, exist near the observation range. As a result, we thereafter considered only dry snow and dry graupel as precipitation particle types. A previous study showed that the threshold of Z_h was 33 dBZ to distinguish the predominant particles in the volume between dry snow and dry graupel. The ratio whose Z_h was larger than 33 dBZ was 11% in these two days. Negative specific differential phase (K_{DP}) increases in the area whose Zh is larger than 30 dBZ (Fig. 5). This result indicates that the ratio of conical graupel, which falls at the vertically oriented attitude, increases.

The polarimetric radar observation in Hokuriku shows a potential to obtain detailed information about solid precipitation particles. To clarify the difference in cloud precipitation mechanisms, further observation should be performed in other locations. In addition, quantitative precipitation estimation of each precipitation type remains to be an important problem.

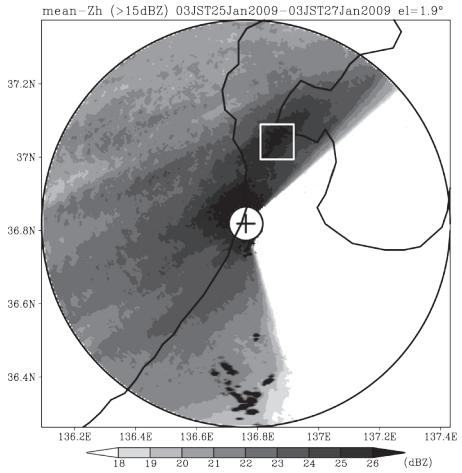

Fig. 4 Time-averaged reflectivity pattern in the radar observation range at 1.9 degree elevation angle from 03 JST on January 25, 2009 to 30 JST on January 27, 2009. The white square shows the region in which frequency of polarimetric parameters is examined.

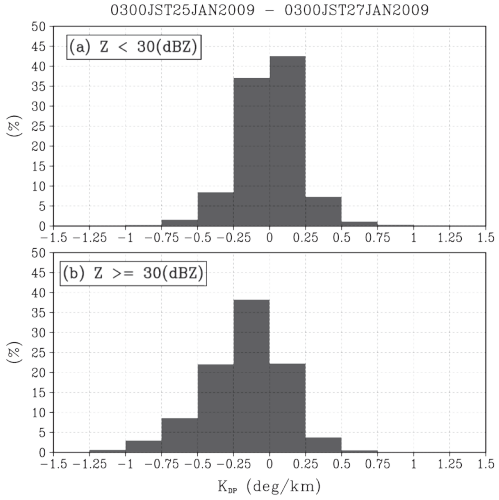

Fig.5 Frequency of specific differential phase (K_{DP}) in the snowfall enhancement region: (a) for grids whose Zh is less than 30 dBZ and (b) for grids equal to or larger than 30 dBZ.

Formation and maintenance mechanisms of a stationary snowband along the Hokuriku Coast in prevailing westerly

During the cold-air outbreak, a stationary snowband is occasionally observed over the Sea of Japan along the San-in-Hokuriku coast, which brings heavy snowfall near the coastal area of Hokuriku District, accompanied with a southerly offshore wind. A convergence zone that causes the formation of the snowband is observed between the southerly and westerly environmental flow. However, the mechanisms that form the southerly offshore wind are not clear. This study examines the formation mechanism of the southerly offshore wind using a Doppler radar and the Cloud Resolving Storm Simulator (CReSS).

Eight cases of stationary snowband formation along the San-in-Hokuriku coast were found in the six winter seasons from December 2003 to March 2009. Strong westerly or west-southwesterly prevailed in the lower atmosphere in all cases. This wind field was different from the ordinal northwesterly monsoon.

We performed numerical simulations using the CReSS for the stationary snowband that developed from January 24 to 26, 2009. The simulation well reproduced the precipitation amount and location of the snowband in comparison with the Japan Meteorological Agency (JMA) radar observation (not shown). A convergence zone between the environmental westerly over the Sea of Japan and southerly offshore wind near the San-in-Hokuriku coast was formed in the lower atmosphere. The convergence generated and maintained the stationary snowband along the San-in-Hokuriku coast.

To clarify the cause of the development of southerly offshore wind, sensitivity experiments to remove the land topography, to change roughness over the land surface to that over the sea surface, and to change thermal properties over the land surface to those over the sea surface, were performed. Since the southerly offshore wind was not reproduced in the experiment to change thermal properties, it was mainly formed by the effect of thermal contrast between the land and sea. Figure 6 shows the result of the back-trajectory analysis on the sensitivity experiment with flat terrain. The time series of forces along the southerly offshore wind show the cause of development. The northward component of the pressure gradient force increases as the air parcels approach the convergence zone along the trajectories over the land (Fig. 7). As the air parcel approaches the Hokuriku area, the southerly wind and northward pressure gradient force increase. This increase is caused by a mesoscale high over the Japanese Islands generated by the land-sea thermal contrast. The northward pressure gradient force accelerates the air parcels toward the north.

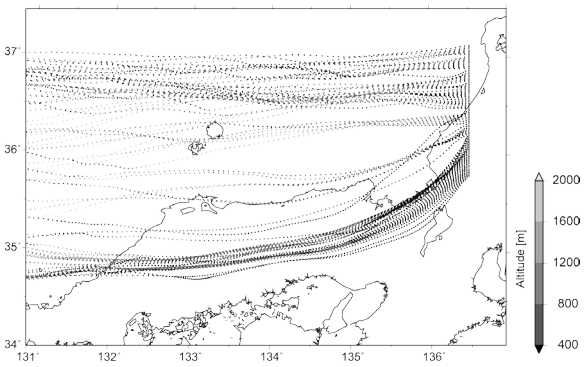

Fig. 6 Back-trajectory analysis on the result of sensitivity experiment with flat terrain. Tracks from 02 JST January 25, 2009 show a course of 12 h.

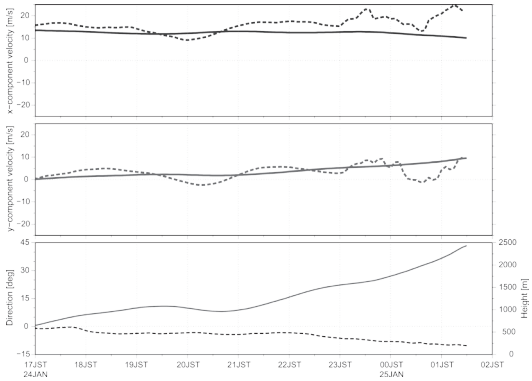

Fig. 7 Time series of velocity (solid line) and geostrophic component (dashed line) of an air parcel that begins at the south side of the convergence zone. The upper and middle panels show the zonal and meridional components, respectively. The lower panel shows time series of wind direction (solid line) and height (dashed line) of the air parcel.

Evaluation of the snow/graupel ratio of the simulation results using the CReSS based on ground-based observation

To evaluate cold rain processes, such as the conversion process from snow to graupel, in the CReSS, we compared the snow/graupel ratio at the ground simulated by the CReSS with the results obtained by the ground-based particle observation system of Kanazawa University.

The ground-based particle observation system takes a picture of each solid particle, digitizes it by an image processing technique, and archives the shape, diameter, and falling speed of each particle. The number concentration of particles is also archived. The complexity, which is the ratio of length of the circumference to that of minimum area, and number of holes are utilized to evaluate whether the particle is a snowflake or graupel. The total volume of snowflakes and graupel is calculated as the sum of particle volumes achieved by rotating particle area. The total volume is gathered every minute.

We performed daily simulations over almost the entire Sea of Japan with a horizontal grid resolution of 5 km and near Ishikawa Prefecture with 1 km from December 24, 2008 to April 7, 2009, using the CReSS. The snowfall and graupel-fall amounts obtained from the simulation at the grid of Kanazawa University (136.71E, 36.55N) were compared with those obtained from the ground-based particle observation system. The evaluation of volume ratio between snowfall and graupel-fall was conducted during the four days (January 13, 15, and 24, and February 16, 2009) when the particle observation system was operated.

Figure 8 shows the time series of the accumulated volume of snowfall and graupel-fall at each minute obtained from the ground-based particle observation system at Kanazawa University and the data obtained from the CReSS with a 1-km horizontal grid resolution. Precipitation amounts of snowfall and graupel-fall directly correspond to the volume of each particle by assuming unit area. Spontaneous increases of accumulated volumes of snowfall and graupel-fall appear in the ground-based observation, and correspond to the passage of precipitation cells. Although both snowfall and graupel-fall are found in the ground-based particle observation, almost all precipitation is caused by graupel-fall in the simulation. Figure 9 shows a scatter plot of the ratio of graupel-fall to the total precipitation between the observation and simulation every hour of the four-day period. As plots are mainly located in the upper-left side, the simulation results overestimate the graupel-fall ratio compared with the observation. This result indicates the tendency to excessively generate graupel in the cold rain parameterization used in the CReSS.

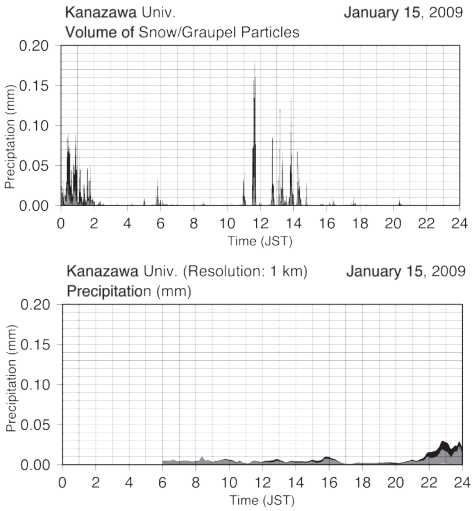

Fig. 8 Time series of accumulated volume of snowfall (black bar) and graupel-fall (gray bar) at each minute obtained from the ground-based particle observation system at Kanazawa University (upper panel) and that obtained from the CReSS with 1-km horizontal grid resolution (lower panel).

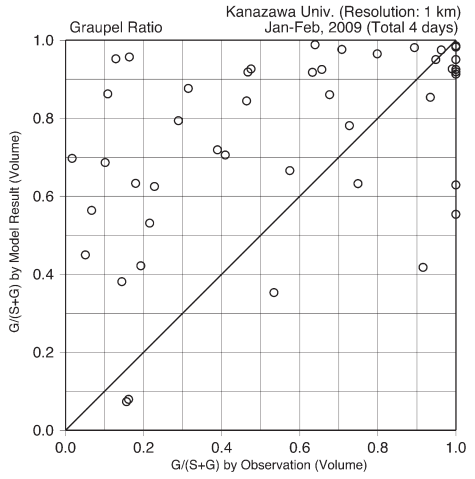

Fig. 9 Scatter plot of the ratio of graupel-fall to total precipitation (snowfall plus graupel-fall amount) between the observation in the horizontal axis and simulation in the vertical axis. Each plot indicates accumulated values every hour during January 13, 15, and 24, and February 16, 2009, when the particle observation system was operated.

Simulation of tornado-scale vortices occurring in winter cold-air outbreak over the Sea of Japan

Tornado-scale intense vortices, including tornadoes and waterspouts, called "Tatsumaki" in Japanese, occur below intense convective clouds. Two major types of tornado-genesis are known: a supercell type and a non-supercell type along a meso-front. Niino et al. (1997) showed that a majority of tornadoes occurs in coastal regions of Japan and about 12% of tornadoes are associated with the winter monsoon. When a cold-air outbreak occurs over the Sea of Japan, shallow convective clouds develop and are usually ordinary cells with a short lifetime. Since the Tatsumaki in the winter monsoon occurs over the sea and its life time is short with their small scale, there are almost no reports about the Tatsumaki in the coastal regions of the Sea of Japan except Kobayashi et al. (2007). They observed Tatsumaki in the coastal region using a Doppler radar and photographs, and showed its horizontal scale of 150 m at a height of the cloud base.

On December 25, 2005, a train accident caused by a strong gust wind occurred in the coastal region, and five people were killed. The Tatsumaki is the most probable phenomenon of wind gust associated with a snowstorm. A high-resolution numerical simulation is a possible approach to clarify the characteristics and structure of the Tatsumaki in a snowstorm. Since the horizontal scale of the Tatsumaki is as large as 100 m, a very high resolution of several tens of meters is necessary, and the computation is very large. A huge parallel computer named the Earth Simulator makes large simulations of the Tatsumaki possible.

In our study, an one-way triple-nesting technique was used for the high-resolution simulation of intense vortices of the Tatsumaki with three different horizontal resolutions of 2000 m, 250 m, and 50 m, respectively. The initial and boundary conditions were provided by the forecast model output data of the JMA, and the initial time was 00 UTC, December 25, 2005. The domains are shown in Fig. 10. The simulation of 50 m resolution was performed for 2.5 h. A cold-air outbreak occurred over the Sea of Japan, and the front of the cold air pushed the warm and moist southwesterly wind toward the southeast. A large number of shallow convective clouds with intense vortices of both positive and negative vorticity developed in the cold air of the winter monsoon. A typical vortex with positive vorticity is shown in Fig. 11. Both vortices have an absolute vorticity of about 0.3 s^{-1}, maximum wind speed of about 30 m s^{-1}, and horizontal scale of about 200 m. This is close to the scale of the winter tornado observed by Kobayashi et al. (2007). The velocity field of both vortices is balanced with the pressure field, that is, the cyclostrophic balance.

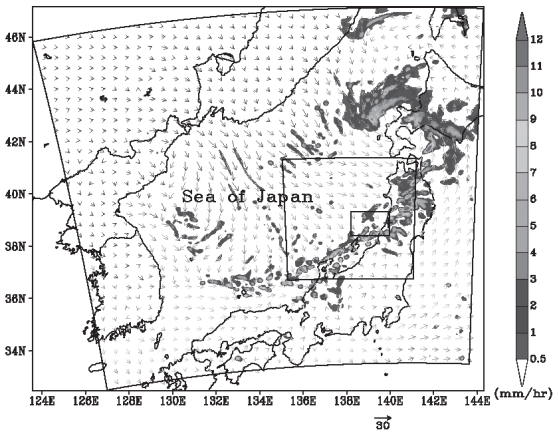

Fig. 10 Computational domains for the triple-nested simulation experiments. The outermost, middle, and innermost regions are those of 2000 m, 250 m, and 50 m resolution simulations, respectively. Shadings indicate rainfall intensity obtained from the 2000 m resolution simulation.

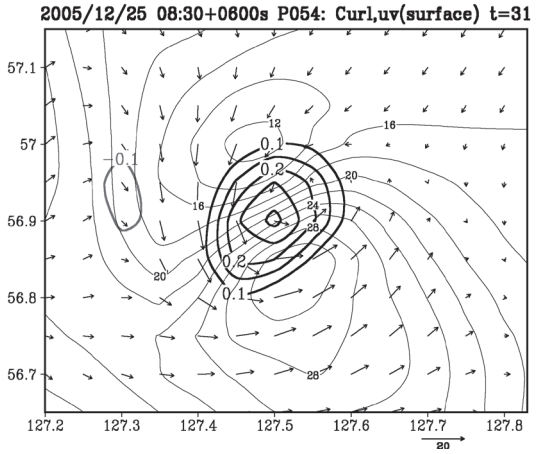

Fig. 11 An example of a typical vortex with positive vorticity. Thick and thin contours indicate vorticity and wind speed at the surface, respectively. The arrows indicate horizontal wind vectors at the surface.

Laboratory for Climate System Study

Changes in the Asian monsoon climate during 1700–1850 induced by preindustrial cultivation

Monsoon is generated from a thermal contrast between land and ocean. Thus, the land's surface condition is an important factor in determining its climate. Monsoon Asia, where >50% of the world population is concentrated, has experienced large land cover/use changes due to agricultural development, particularly during the 18th and 19th centuries. In India and China between 1700 and 1850, extension of cultivation and habitation activities decreased the percentage of forested area from 40–50% to 5–10% of the entire territories between 1700 and 1850. Changing the land cover/use from forest to croplands can affect the global and regional climate through changes in the energy and water balance at the earth's surface. Among the various effects of vegetation change, 2 factors have been shown to have a major influence on the energy and water balance: (i) an increase in surface albedo leading to a reduction in solar energy absorption at the surface and (ii) a decrease in surface roughness, resulting in low-level wind speed intensification. As a consequence, the partitioning of turbulent heat fluxes into its sensible and latent heat fluxes would subsequently affect the planetary boundary layer and deep cumulus convection and, hence, the large-scale atmospheric phenomena.

We examined the actual impacts of land cover/use changes using a global historical vegetation map reconstructed for the last 300 years. In the first half of the period, from 1700 to 1850, intensive cultivation activities continually occurred over the Indian subcontinent and over eastern China in Asia (shaded areas in Fig. 1). Croplands in India have continued to increase since the 17th century when the British East India Company embarked on the colonial management in the Mughal Empire. Croplands expanded explosively in China in the 1700s in response to the introduction of new crops (e.g., corn, sweet potato, peanut) and to the rapid increase in population under the favorable economic policies of the Qing Dynasty. We considered that the difference between the climatic realizations of the 2 periods, in the 1700s and in the 1850s, might represent the long-term changes that occurred in those 150 years, and we examined the impacts of the reconstructed historical land cover/use changes between those 2 periods. Consequently, we conducted 2 time-slice numerical experiments for the periods represented by 1700 and 1850, using the historical vegetation maps of 1700 and 1850 as the lower boundary conditions for an atmospheric general circulation model (AGCM), considering the changes in physical and physiological parameters of vegetation. Both equilibrium experiments were repeatedly forced by identical climatological annual cycles of the present-day monthly distributions of sea surface temperature (SST) and sea ice. The averaged states of summer (June, July, and August) we recomputed for the equilibrated results. These were compared for examining the impact of the land cover/use changes on the Asian summer monsoons between the 2 periods (Takata et al., 2009).

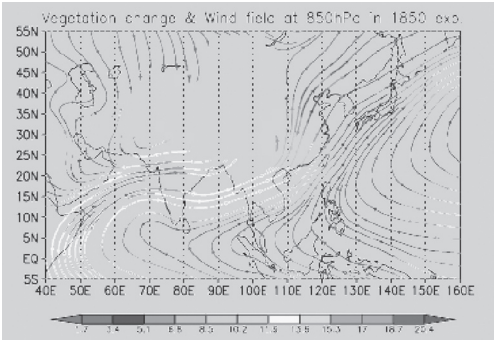

Fig. 1. Land cover/use changes between 1700 and 1850 (gray shades) and 850-hPa wind in June–August (streamlines with colors in meterss^{-1}) in the 1850 experiment (Takata et al., 2009)

Changes in Wind Field and Surface Energy–Water Balance Between 1700 and 1850.

In the western Indian subcontinent and in southeastern China, the summer monsoonal wind blows from the ocean to the land in the lower troposphere (streamlines in Fig.1). Because winds usually decelerate over land because of the large surface roughness, atmospheric moisture convergence and, hence, precipitation are large in those regions. Most of the agricultural cultivation during 1700–1850 occurred on forest, causing the surface roughness to de-

crease because of the reductions in vegetation height and leaf amount[specified as leaf area index (LAI)]. As a result, the surface wind troposphere as seen in the changes in 850-hPa wind field (arrows in Fig. 2A), which resulted in a reduction in the moisture convergence and the precipitation in the western Indian subcontinent (hereafter the IND region) and in southeastern China (hereafter the SCH region) (Fig. 2B). The reduction in precipitation reduced the surface soil moisture and, hence, the local evaporation and moist convection, creating a positive feedback to further precipitation reduction. A vegetation change from forest to cropland resulted in an increase in the surface albedo (colors in Fig. 2C) due to the decrease in LAI and the increase in leaf reflectivity. However, effects of the increase in surface albedo were overshadowed by a decrease in clouds in the IND and SCH regions associated with the significant decrease in precipitation. As a result, net shortwave radiation (i.e., absorbed at the surface) was increased, and the decrease in soil moisture was further enhanced in those regions (contours in Fig. 2C). On the other hand, net short-wave radiation was decreased in the middle of eastern China (hereafter the ECH region) because of the increase in surface albedo. The decrease in net short-wave radiation caused a decrease in surface temperature but only in part of the ECH region where surface soil moisture was not decreased).These decreases would have less effect on precipitation change.

Changes in Atmospheric Water Balance.

Our results suggest that the atmospheric water balance in those regions reflects whether surface roughness reduction and albedo increase had a majorrole in the summer climate change. In the IND and SCH regions, the ratio of moisture convergence to the source of precipitation was high. In those regions, the moisture convergence changed considerably due to a combined effect of the decreased surface roughness and the decreased soil moisture. However, in the ECH region, dependence on the

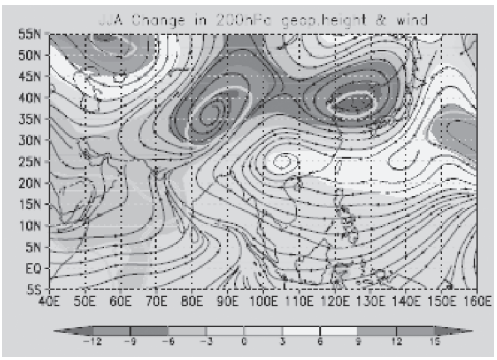

Fig.3. June–August mean changes in the 200-hPa wind field (streamlines)and geopotential height (colors, in meters) between 1700 and 1850. Thick gray lines represent those in which the differences are statistically significantat the 95% confidence level (Takata et al. 2009).

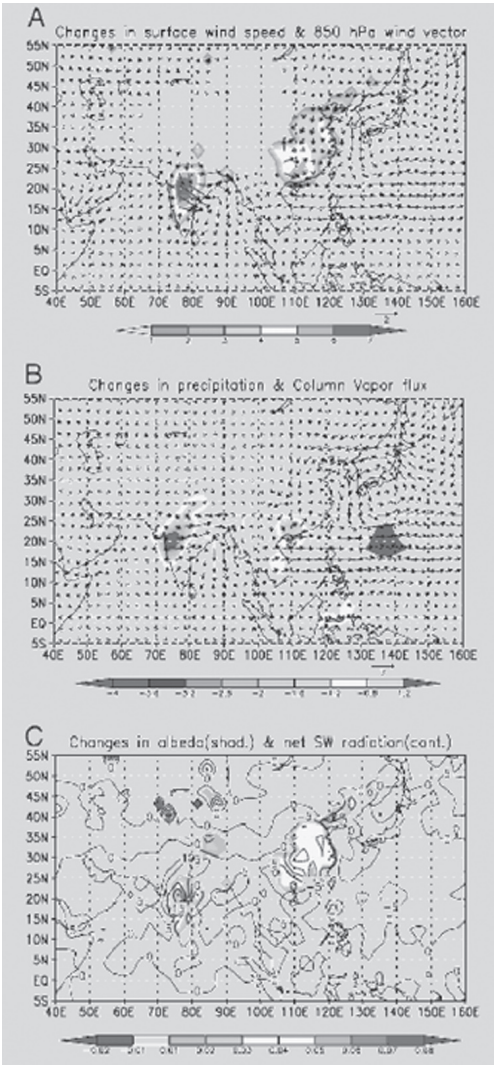

Fig.2. June–August mean changes between 1700 and 1850. (*A*) Surfacewind speed (colors, in m s^{-1}) and 850-hPa wind (vectors, with unit vector 2 ms^{-1}). (*B*) Precipitation (colors, in mm day^{-1}) and vertically integrated vapor flux(vectors, with unit vector 7 – 10 kg m^{-1} s^{-1}). (*C*) Surface albedo (colors, unit of legends is nondimensional) and net short-wave radiation absorbed at the surface (downward positive; contours, with labels in Wm^{-2}). Shaded regions are similar to those where the differences in surface wind speed, precipitation, or surface albedo are statistically significant at the 95% confidence level (Takata et al. 2009).

moisture convergence was low, and precipitation changed little. Thus, the albedo effect, in terms of reducing net short-wave radiation (contours in Fig. 2C), was more apparent in this area.

The changes in precipitable water for the June–August mean were very small and negligible in each region and each time period (less than a few millimeters. Month-1). As a result of the overall changes in precipitation and atmospheric heating induced by agricultural development particularly in south and southeast Asia, the Tibetan anticyclone in the upper troposphere weakened in 1850 (Fig. 3) The weakening of the Asian summer monsoon by cultivation was also interpreted by using a regional climate model. The North Pacific high weakened in 1850, which was associated with the weakened Tibetan anticyclone. This weakening of the North Pacific high resulted in the slight increases in moisture convergence and precipitation in the ECH region, in contrast to the decreases in those in the IND and SCH regions

reference: Takata, K., K. Saitoh and T. Yasunari (2009): Changes in the Asian monsoon climate during 1700–1850 induced by preindustrial cultivation. Proc. Nat. Acad. Sci. U.S.A., doi:10.1073/pnas.0807346106

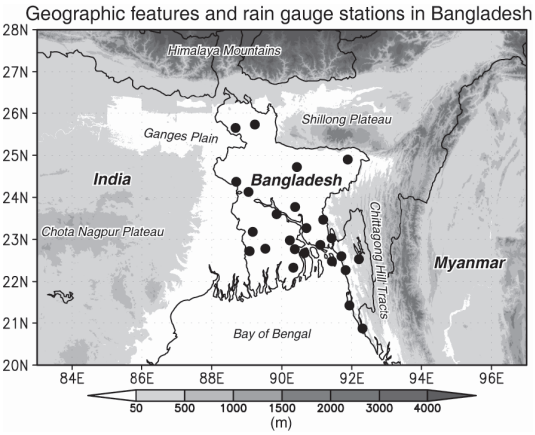

Fig.4. Geographic features in and around Bangladesh. Closed circles denote the locations of the 25 rain-gauge stations used in this study.

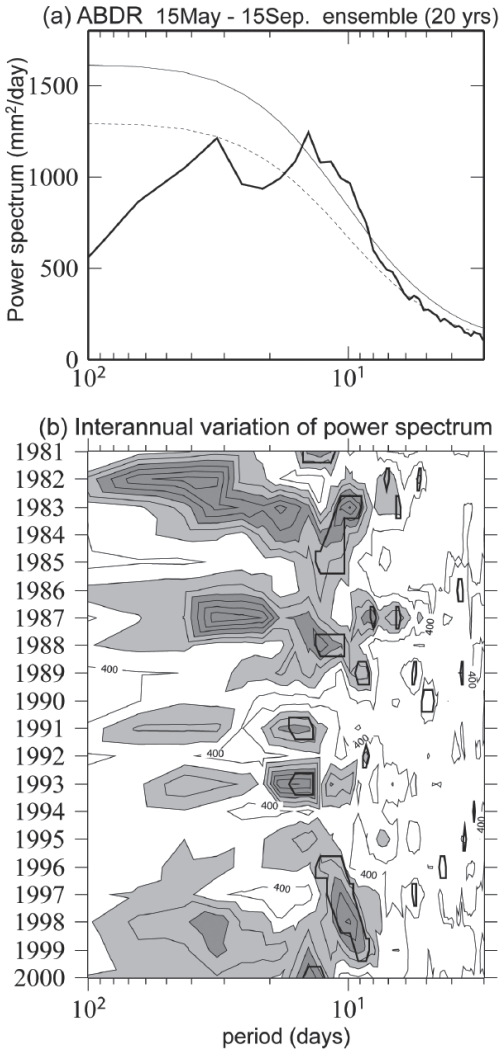

Fig.5. (a) The 20-summer ensemble spectrum of rainfall time series from 15 May to 15 September (124 days) over Bangladesh. . (b) Interannual variation of the ABDR spectrum from 1981 to 2000.

Intraseasonal oscillation of rainfall and its effect on interannual variability over Bangladesh during boreal summer

The Intraseasonal oscillation (ISO) of rainfall during the summer monsoon season (June–August) and its possible effect on the IAV of total summer monsoon rainfall over Bangladesh were examined using daily rainfall data from 25 rain-gauge stations for 20 years (1981–2000) (Fig. 4). The rain-gauge data for each of the 25 stations were simply averaged for each day

(defined as the 'all Bangladesh daily rainfall' and abbreviated as ABDR). The space–time structures of atmospheric circulation and large-scale convection fields related to the ISO and the IAV of the ABDR were also investigated using Japanese 25-year reanalysis (JRA25) and interpolated OLR data. The analysis using multiyear rain-gauge data from a dense observation network revealed robust and characteristic features of the ISO climatology in Bangladesh.

An ISO of 7–25 days (submonthly scale) appears in the ABDR time series in almost all of the 20 years (1981–2000) (Fig. 5). The variance shows a large IAV. In contrast, the activity of 30–60-day ISO is weak and spectral peaks occasionally appear in this period range. The 7–25-day filtered ABDR variance is always very large compared with the 30–60-day variance (Fig. 6). Thus, submonthly scale ISO can be regarded as a dominant intraseasonal mode of rainfall fluctuation over Bangladesh during the summer monsoon season.

The time evolution of atmospheric circulation and convention anomalies associated with submonthly scale ABDR ISO reveals that the changes in atmospheric circulation over the Bay of Bengal are associated with the so-called synoptic-scale 10–20-day ISO that originates around the western Pacific and then moves westward to India. In the peak active phase, active convection anomalies appear over northeastern India, all of Bangladesh, and western Myanmar, whereas suppressed convection anomalies occur over the southern Bay of Bengal, accompanied by a cyclonic anomaly from northeastern India to northwestern Myanmar, centered on northern Bangladesh, and an anticyclonic circulation anomaly over the central Bay of Bengal (Fig. 7). Note that despite the continuous westward migration of convection and circulation anomalies over the Bay of Bengal, the convection anomalies and cyclonic anomalies over Bangladesh remain in almost the same location from the initiation to termination of the active ISO phase.

The spatial patterns of atmospheric circulation and convection associated with the ISO and the IAV are quite similar to each other around the monsoon trough, especially from northeastern India to Bangladesh. Climatologically, Bangladesh is one of the most predominant areas of submonthly scale ISO; however, 30–60-day ISO is not prominent. These characteristic features probably allow the submonthly scale ISO to modulate the total seasonal rainfall and the spatial patterns of circulation and convection over and near Bangladesh.

reference: Fujinami et al. 2010: Characteristic intraseasonal oscillation of rainfall and its effect on interannual variability over Bangladesh during boreal summer, *Int. J. Climatol.*, in press)

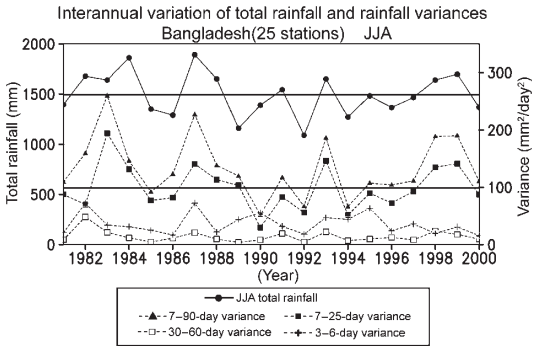

Fig.6. Interannual variations of total ABDR and intraseasonal ADBR variances on intraseasonal timescales and 3- to 6-day ABDR variance for June–August.

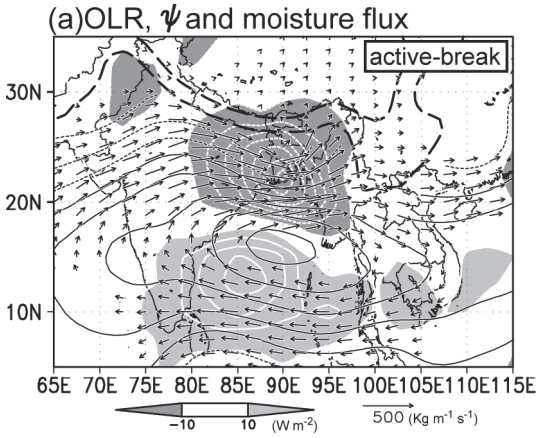

Fig.7. Composite differences of (a) OLR (shadings), 925-hPa streamfunction, and vertically integrated moisture flux vectors between peak active and break phases of 7- to 25-day rainfall variation over Bangladesh.

Laboratory for Cloud and Precipitation Climatology

Development and Improvement of the Satellite Data Simulator Unit (SDSU)

The Satellite Data Simulator Unit (SDSU) is a Fortran package used to compute synthetic satellite data from user-provided geophysical parameters such as cloud-resolving model (CRM) output. As shown in Fig. 1, the SDSU is designed to simulate microwave brightness temperature, radar reflectivity, and visible/infrared radiance measured by satellite instruments. The SDSU package also includes a beam convolution routine to adjust the spatial resolution of the CRM to the footprint size of satellite sensors and a Mie lookup table generator to improve computational efficiency.

A primary application of the SDSU is to diagnose the performance of CRMs by comparing CRM-simulated and satellite-observed radiance. Model evaluation studies using a satellite simulator have advantages over using a more traditional approach, based on satellite retrievals such as surface rain rate. As depicted in Fig. 2, a satellite retrieval algorithm is an "inversion model" that inverts satellite measurements to find the input of the radiative transfer problem under several assumptions to characterize underlying uncertainties. In contrast, the SDSU operating as a "forward model" requires no inversion model to be invoked, and is immune to errors arising from satellite retrievals.

The SDSU version 2 (SDSU-v2), the upgraded version of the SDSU as of 2009, includes a new user interface to explicitly characterize the particle size distribution (PSD) model for each hydrometeor species simulated. An adequate characterization of the PSD models is crucial because some satellite sensors, in particular radars, are sensitive to hydrometeor particle size. The SDSU PSD library not only provides pre-installed PSD templates containing conventional microphysical models such as exponential and gamma PSDs, but also enables users to build their own PSD models. The SDSU-v2 can possibly support arbitrary single- and double-moment bulk microphysics schemes. As of March 2010, the SDSU-v2 has more than 40 registered users including many from overseas.

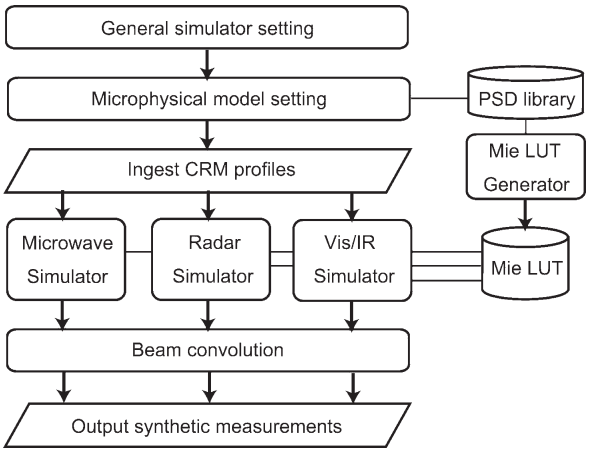

Fig.1. SDSU flow chart.

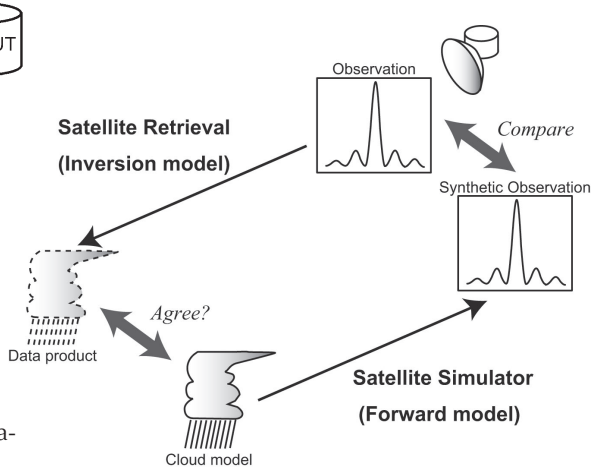

Fig.2. Schematic contrasting a satellite simulator and a satellite retrieval algorithm.

Climate Model Reproducibility of Cloud Radiative Forcing Associated with Tropical Convection

Development of clouds in response to deep convection largely dominates the Earth's radiation budget over the tropics and subtropics. However, it is difficult for climate models to precisely simulate clouds and their impacts on the radiation budget, leading to a large uncertainty in future climate projection. Evaluating the model reproducibility of the cloud radiative forcing (CRF) using observations as the reference is indispensable for further improvement of the climate models. In this study, the CRF simulated by a group of climate models that were included in the International Panel for Climate Change (IPCC) Assessment Report 4 (AR4) is evaluated by focusing on areas with sea surface temperatures (SSTs) higher than 27°C, where deep convection is particularly active. Climate regimes having different dynamical environments are separated in terms of large-scale ascent at the middle troposphere (500 hPa) or ω_{500}, which is used as a proxy for large-scale atmospheric circulation.

The probability distribution function of ω_{500} (Fig. 3) illustrates that strong ascent and weak subsidence dominate the areas with SSTs higher than 27°C. Interestingly, the ratio of shortwave cloud forcing (SWCF) to longwave cloud forcing (LWCF), denoted by N, remains approximately constant in the observation regardless of the ambient large-scale field. On the other hand, the models demonstrate that N increases as the large-scale ascent weakens and eventually turns into subsidence, and thus largely overestimates the observation. The model's incapability to properly simulate the LWCF sensitivity to SST is considered as one of the causes for this overestimation. It is indicated that climate models generally suffer from systematic bias over areas where moist convection is activated by a local thermodynamic regulation against a dynamic forcing unfavorable for convection.

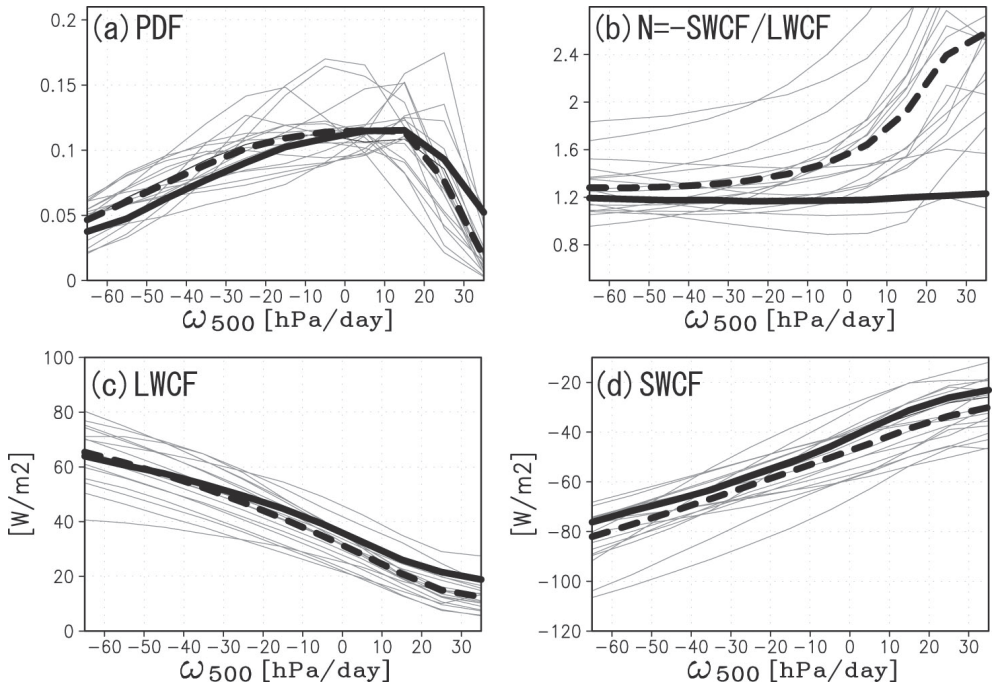

Fig.3. (a) Probability distribution function of ω_{500}, (b) N at 500 hPa level, (c) LWCF at 500 hPa, and (d) SWCF at 500 hPa. Thick solid, thick dashed, and thin lines indicate the observation, model ensemble mean, and individual models, respectively.

Loboratory of Satellite Meteorology

Diurnal variations in summer monsoon precipitation during active and break periods over central India and the southern Himalayan foothills

Diurnal variations in summer precipitation over central India and the southern Himalayan foothills are investigated using Tropical Rainfall Measuring Mission (TRMM) data from July to August since 1998 through 2007. TRMM Precipitation Radar (PR) and Lightning Imaging Sensor (LIS) data are used to further investigate the characteristics of the precipitation. Based on rainfall characteristics in central India, daily TRMM/3B42 (gridded rain data) data are used to determine active (wet) and break (dry) periods. Diurnal variations in rain rate, rain frequency, conditional rain rate, storm height, and occurrence of convective rain are analyzed using TRMM-PR data (0.1° × 0.1° resolution). Diurnal variations in total lightning flashes are analyzed using TRMM-LIS data.

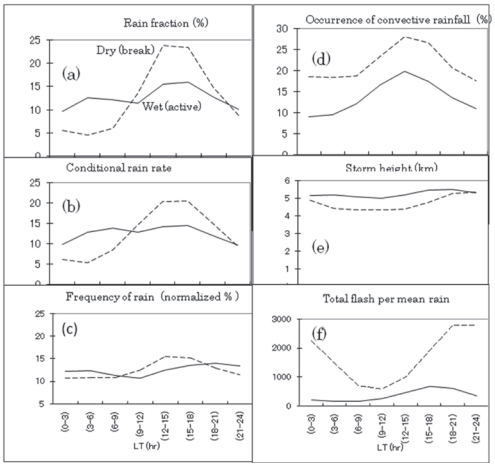

Fig. 1. Diurnal variation in (a) rain fraction, (b) conditional rain rate, (c) rain frequency, (d) occurrence of convective rainfall, (e) storm height, and (f) total flash per mean rain rate during wet periods (solid line) and dry periods (broken line) over central India during the summer.

The precipitation over central India in the active periods is characterized by heavy and frequent rainfall with a secondary morning peak. The precipitation in the break periods is characterized by a strong diurnal variation with isolated convective rain (Fig. 1). Higher temperatures were observed during the dry periods as compared to that during the wet periods. Similar characteristics were observed over the southern Himalayan foothills.

Study of the precipitation characteristics using meteorological data at the Amazonia Institute before World War II

Amazonia plays an important role in global hydrological circulation. It constitutes one-third of the largest area of tropical rain forests left on the Earth. Amazonia includes the Amazon River system; the largest river system on Earth, which carries approximately 20% of all the freshwater that is discharged into the oceans. Before World War II, only a few meteorological observation stations existed. Thus, it is difficult to study the past climates of Amazonia. Before World War II (1931 to 1941), Japanese immigrants in Amazonia recorded meteorological data at the Amazonia Institute. Data recorded from this station are analyzed and discussed here. The data clearly outline the differences between the wet and dry seasons. Temperature varies with the rainfall; lower temperatures were recorded during the rainy season as compared to that during the dry season. A diurnal temperature variation is observed with temperatures being the highest during daytime and lower in the mornings and evenings. The recorded surface wind data also indicate a diurnal variation. The diurnal variation is not seen in the eye observation data for moving direction of clouds. This suggests that the diurnal wind variation exists only in the surface winds. Although there is little precipitation, the frequency of thunder normalized to the amount of precipitation is high in the dry season.

The rainfall distribution maps obtained from TRMM are used to investigate the seasonal movement of the precipitation area. This movement is found to be consistent with the data obtained from the Amazonia Institute as well as the other station. The TRMM data also indicate that the Amazon River affects the diurnal variation of rain. A reason for this could be the river breeze generated due to the land–river thermal contrast.

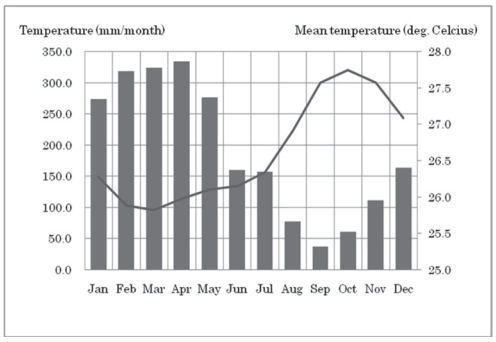

Fig. 2. Monthly mean temperature (red) and amount of rainfall (blue) for 1931–1939.

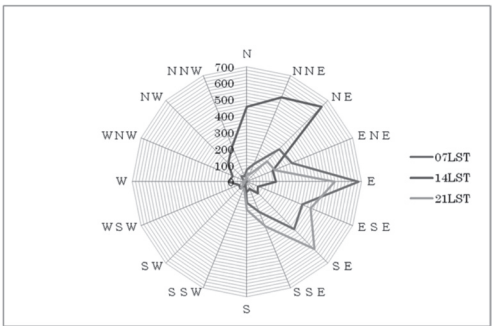

Fig. 3. Wind direction frequency (days) for 1932–1939.

Planning of field experiments conducted for the development of the Global Precipitation Mission dual-frequency precipitation radar algorithm using a dual Ka-radar system

Field experiments conducted for the development of the Global Precipitation Mission (GPM) dual-frequency precipitation radar (DPR) algorithm using a dual Ka-radar system are described below. The parameters that are to be measured in the ground experiments depend on the DPR algorithm. For liquid precipitation, raindrop-size distribution is the primary parameter to be measured. For the dry snow, another parameter of the snow particle density should be measured. For the wet snow or melting layer region, other parameters such as the melting ratio should be measured.

The dual Ka-band radar system, which is being developed by the Japan Aerospace Exploration Agency (JAXA), will be a powerful tool to measure the parameters or their proxies required to develop the DPR algorithm. The dual Ka-radar system can measure both the specific attenuation and the equivalent radar reflectivity at Ka-band. The basic idea is the retrieval of specific attenuation using the symmetrical appearance of rain attenuation in two radars in the same radio path but with the opposite (face to face) direction. Using the dual Ka-radar system along with other instruments (e.g., a polarimetric precipitation radar , a windprofiler radar, and ground-based rain measurement systems), the uncertainties of the parameters required in the DPR algorithm can be reduced. The verification of the improvement of rain-retrieval data using the DPR algorithm is also included as an objective. The experimental plan was investigated as a collaboration study with JAXA. The planned field experiments include: (1) the polarimetric Doppler radar observations at the Okinawa Subtropical Environment Remote Sensing Center, the National Institute of Information and Communications Technology (NICT), (2) snow observations at the Snow and Ice Research Center, National Research Institute for Earth Science and Disaster Prevention in Nagaoka, (3) observations at Kanazawa University, and (4) observations with Hokkaido University in Sapporo City. The experiments also include a melting layer measurement at the slope of Mt. Fuji.

Interpreting space-borne radar observations of shallow convection using a rain-cell model

Observations of shallow, isolated convection obtained from the PR aboard the TRMM satellite were compared to simulations obtained from a rain-cell model to examine the effects of the sub-resolution scale convection on the space-borne radar observations.

High-resolution observations of shallow, isolated convection from the PR agreed reasonably well with the data generated by an idealized model. A large sample of shallow, isolated convection was obtained from the PR data over the central Pacific Intertropical Convergence Zone. The PR field-of-view (FOV) was modeled by a bivariate Gaussian distribution, and the sub-resolution scale rain cells were assumed to be circular and having a constant radar reflectivity (dBZ) value. Cell diameter and cell depth were related by assuming an aspect ratio of 2 (diameter/depth). The average cell dBZ was assumed to be 32 with a standard deviation of 2 dBZ. The comparison of observed and simulated probability distributions of dBZ was favorable, suggesting that the outlined exploratory approach could be useful for estimating the rainfall rate retrieval errors caused by the nonlinearities between the radar reflectivity and the rainfall rate and partially filled FOVs.

Laboratory of Eco-Hydrometeorology

Estimation of ecosystem respiration over a paddy field using storage change in CO_2 density in the nocturnal boundary layer

Accurate estimation of terrestrial ecosystem respiration is crucial for developing regional- to global-scale carbon-budget databases. This study evaluates nighttime ecosystem respiration under low-turbulence conditions in a paddy field in China during the 2004 growing season. Data from turbulent flux with storage change in CO_2 density, and alternatively from CO_2 concentration profiles measured from the surface to a height of 32 m, were investigated and compared (Fig. 1). Conditions were separated into windy and calm according to where they fell with respect to friction velocity (u_*) threshold. On calm nights, the vertical gradient of CO_2 concentration is higher near the canopy level and decreases with height. No differences are detected in the quantity or seasonality of nighttime ecosystem respiration (*Re*) between values observed by eddy covariance and values calculated under calm conditions. Underestimation of nighttime *Re* values is low, even under calm conditions. Under stable conditions, nighttime CO_2 flux is small, perhaps mainly because CO_2 is stored in air below the sensor height; similarly, CO_2 drainage loss is small, perhaps because advection is small. The addition of measurement-height storage change in CO_2 density helps reduce underestimation of nighttime *Re* values, so u_* filtering and elimination of low-turbulence data are not required for a paddy ecosystem. In contrast, under low-turbulence conditions, nighttime flux can be calculated from concentration profiles, but actual measurement of the height of the nocturnal boundary layer is very important. To fill gaps in nighttime CO_2 flux data for a paddy ecosystem, development of multiple regression functions based on the crop-biomass/leaf-area index in association with field water status is preferable to development of just a single regression function based on air/soil temperature.

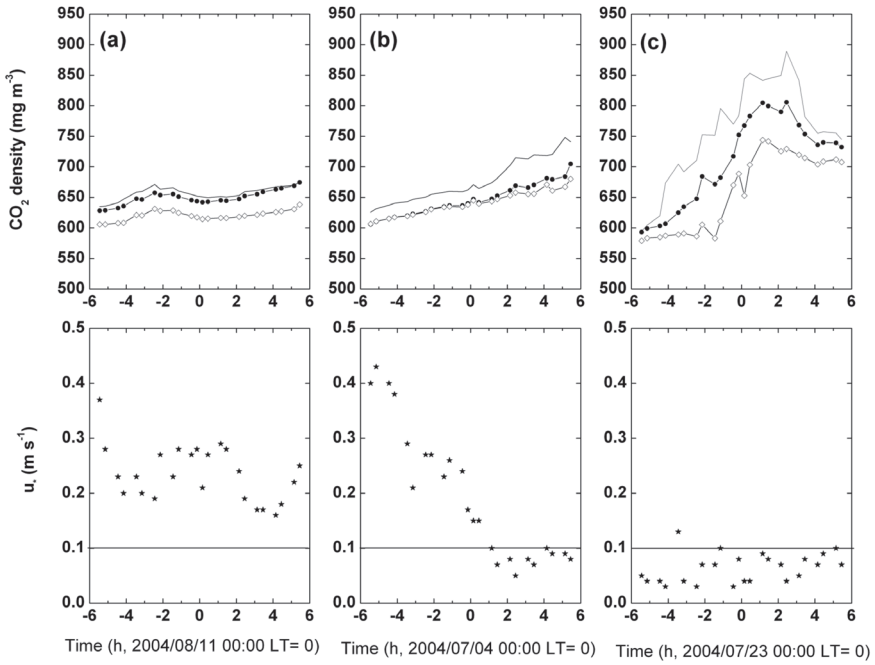

Fig.1. Nighttime CO_2 density and friction velocity (u_*) for (**a**) windy, (**b**) intermittent, and (**c**) calm nights; the symbols represent the following: —, 3.5 m height; •, 12.2 m height, and ◊, 32 m height.

Estimation of regional CH_4 flux over a paddy field using storage change in CH_4 density in the nocturnal boundary layer

This study observes the nighttime inversion layer over a paddy field in summer and evaluates methods for estimating regional methane flux over such a field. On July 13, July 16, and August 4, 2009, we performed tethered-balloon observations of nighttime inversion layers over a paddy field in Tsukuba, Ibaraki, Japan. Analysis of vertical profiles for CH_4, CO_2, potential temperature, relative humidity, wind direction, and wind speed from the surface to heights of several hundred meters revealed the presence of nighttime inversion layers (Fig. 2). A previous method for evaluating regional CH_4 flux using chambers (the so-called chamber method) proved insufficient, hence we tried a method using a time series of CH_4 profiles beneath the nighttime inversion height, hereafter called the inversion-layer storage method (ILSM). For comparison, we also obtained regionally measured CH_4 and CO_2 fluxes evaluated by the gradient method (GM) and the eddy covariance method (ECM) from the National Institute for Agro-Environmental Sciences (NIAES). Comparison of the various methods indicates that CH_4 fluxes obtained by ILSM (0.41 ± 2.78 $\mu g \cdot CH_4\ m^{-2}\ s^{-1}$) are in good agreement with those obtained by GM (0.55 ± 0.45 $\mu g \cdot CH_4\ m^{-2}\ s^{-1}$). Additionally, CO_2 fluxes obtained by ILSM (510 ± 176 $\mu g \cdot CO_2\ m^{-2}\ s^{-1}$) are overestimated compared with those obtained by ECM (122 ± 43 $\mu g \cdot CO_2\ m^{-2}\ s^{-1}$), but agree within an order of magnitude. Thus we suggest that the ILSM method is suitable for estimating regional CH_4 flux.

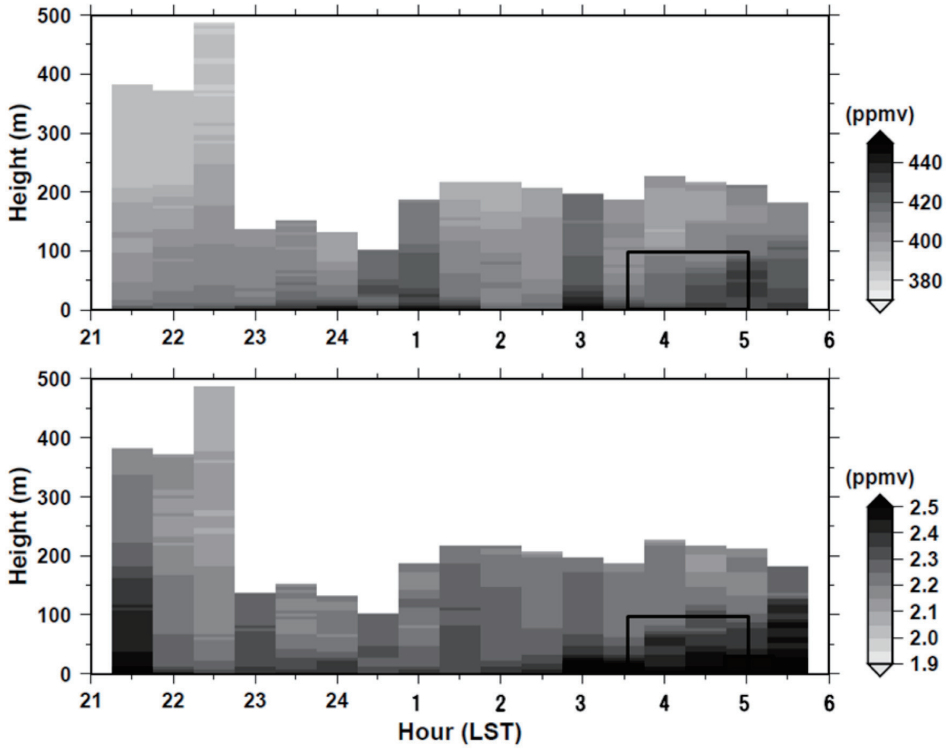

Fig.2. Time–height sections for CO_2 (upper figure) and CH_4 (lower figure) concentration observed from 21:00 JST of 4 August to 06:00 JST of 5 August, 2009. Boxes in these figures indicate target duration and height range used for ILSM.

Laboratory of Satellite Biological Oceanography

Comparison of Primary Production Measured by Carbon and Fluorescence Methods in Ariake Sound

Primary production (PP) in the ocean is usually measured by the rate of assimilation of carbon isotopes (^{14}C or ^{13}C) into particulate matter from bicarbonate ions. However, it is difficult to obtain large data sets because data collection is time consuming. Their accuracy is also questionable because bottle incubation is required for the measurements. A recently developed method of measurement is the use of the fast repetition rate fluorometer (FRRF). This is a simpler and quicker method of measuring PP, and measurements can be taken continuously with deployment of the equipment from vessel and with settling at a moored site. Those methods (rate of carbon isotopes assimilation and FRRF) are fundamentally different; the former measures net PP during incubation, and the latter measures instantaneous gross PP. This study compared the results from both methods in Ariake Sound, Japan, with large tidal amplitude, for understanding the similarities and differences between the methods.

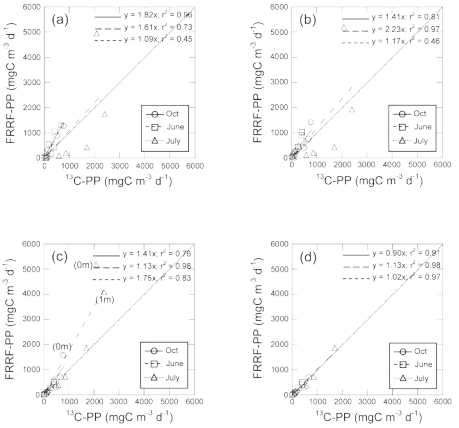

Fig. 1. Comparison of carbon and fluorescence methods for measuring PP at various depths measured by (a) integrating time series of FRRF measurements, (b) implementing incubation chlorophyll-a to calculate PP from FRRF, (c) implementing incubation chlorophyll-a and light conditions to calculate PP from FRRF, and (d) same as (c) excluding the near-surface samples.

PP measurements taken by one-hour incubation using the carbon method were similar to those measured by FRRF, except for those measured at the surface. However, those measured by 24-hour incubation differed significantly from the time-integrated FRRF measurements taken several times daily (Fig. 1). This may be because the samples analyzed using the carbon method were taken at dawn and incubated with the light condition at that time; whereas the fluorescence method measured PP at a stationary location with large fluctuations of phytoplankton abundance (chlorophyll-a) and the light conditions. Using the relationship between light and PP per chlorophyll-a obtained by FRRF with chlorophyll-a concentration and light condition during incubation, the daily PP values measured by carbon and fluorescence methods were similar, except for the surface values (Fig. 1). This indicates that water mass movement by tidal motion may be the cause of the discrepancy. It was also possible to calculate the daily PP using a single FRRF cast data around noon, the period with highest light intensity, with the relationship between light and PP per chlorophyll-a.

There are still some uncertainties about the surface area values, which may include errors in both carbon and FRRF methods, and about the difference of net and gross PP. However, the FRRF method can be used to obtain PP data easily, and when combined with satellite data, it is expected to estimate accurately the PP of marine environment, including that of coastal areas.

Ten-Year Seasonal and Interannual Variability of Satellite Chlorophyll-a in the East China Sea

Recently, environmental changes, such as frequent occurrence of red tide events and giant jellyfish blooms, have been reported in the East China Sea. It has been also suggested that the Three-Gorge Dam (one of the world's largest dams) on the Changjiang River influences the marine ecosystem of the East China Sea. Remote sensing data accumulated over the last 10 years may be able to detect interannual changes in the abundance of phytoplankton (chlorophyll-a), the major primary producer of marine ecosystem. However, the accuracy of chlorophyll-a data measured by a satellite (satellite chlorophyll-a) is known to be poor in this region, and one of the reasons is the presence of high suspended matter. Seasonal and interannual variability of standard satellite chlorophyll-a products in the East China Sea and the Yellow Sea were studied in this study with taking into account the possible error of the satellite chlorophyll-a.

Data indicate that the satellite chlorophyll-a data averaged over 10 years was high over the nearshore areas of the East China Sea, the Yellow Sea, and the Bohei Sea; and low over the open ocean (Fig. 2). High satellite chlorophyll-a region was also observed in the middle of the East China Sea, from the mouth of the Changjiang River to the east. This high satellite chlorophyll-a area corresponded to the shallow area extended eastward during winter; however it did not follow the bottom topography, during the summer months when the discharge from the Changjiang River was at a maximum. Indicator of suspended matter, normalized water leaving radiance of 555 nm (nLw555), was high in the nearshore area and high satellite chlorophyll-a area at the east of Changjiang mouth during winter (Fig. 2). It was suggested that satellite chlorophyll-a was overestimated in the high nLw555 area, the nearshore area and the east of Changjiang mouth during winter. On the other hand, during summer in the middle of the East China Sea, satellite chlorophyll-a and nLw555 were high and low, respectively. The high satellite chlorophyll-a was caused by the increase of chlorophyll-a with relation to the Changjiang River discharge.

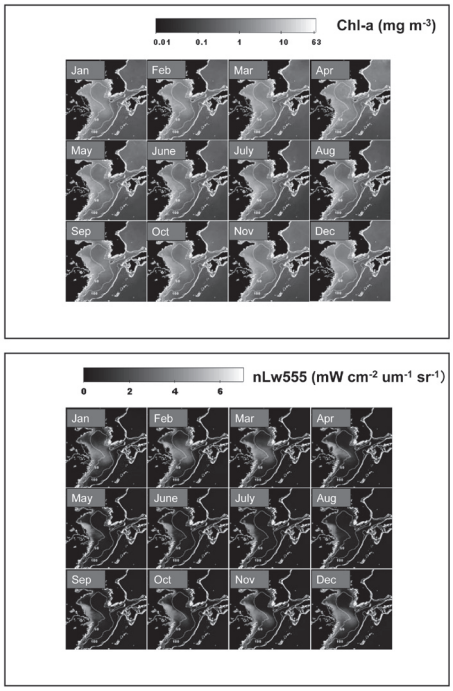

Fig. 2. Distribution of 10-year averaged monthly satellite chlorophyll-a (upper) and nLw555 (lower). White lines indicate bathymetry at 50 m intervals.

A seasonal maximum of satellite chlorophyll-a was observed from March to April south of the East China Sea to the Yellow Sea. This may correspond to the spring bloom of phytoplankton that is typically seen in the coastal temporal area (Fig. 3). Satellite chlorophyll-a data from the mouth of the Changjiang to the Tsushima Strait showed another peak in summer, thus indicating the influence of summer discharge from the Changjiang River. This peak shifted from the mouth of the Changjiang in June–July to the east of Cheju Island in August–September with a decrease in its magnitude. The summer peak of satellite chlorophyll-a showed that interannual variability correlated to that of the summer discharge of the Changjiang River, with a 0–2 month's time lag (Fig. 4). In the Yellow Sea, the relationship between the Changjiang River discharge and satellite chlorophyll-a was not clear, and satellite

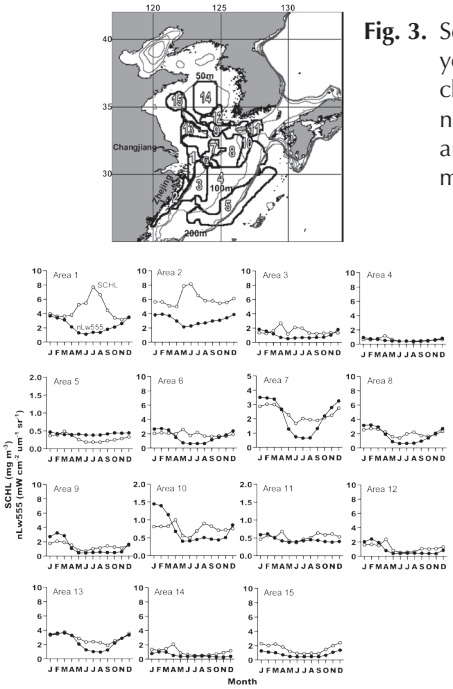

Fig. 3. Seasonal variation of 10-year averaged surface chlorophyll-a (open) and nLw555 (closed) in each area shown in the upper map.

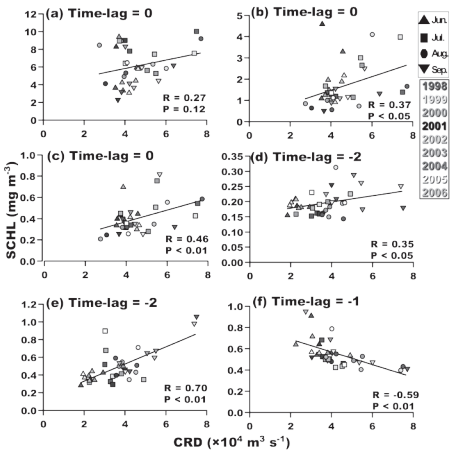

Fig. 4. Scatter plot of monthly chlorophyll-a from June to September and the Changjiang River discharge with a 0–2 month's time lag for areas 1 (a), 3 (b), 4 (c), 5 (d), 11 (e), and 14 (f). Time lag indicates the month of satellite chlorophyll-a following the month of the Changjiang River discharge.

chlorophyll-a gradually increased over the 10 years.

It was apparent that there is a strong relationship between phytoplankton abundance and the Changjiang River discharge in the middle of the East China Sea, and that this discharge is the major factor controlling primary production. This indicates that primary production in the East China Sea will change radically if there is a significant change in the Changjiang River discharge caused by a climatic change and/or other human activities. It also indicates that the East China Sea is directly influenced by the discharge of the Changjiang River, where the Yellow Sea may be more influenced by eutrophication of the Changjiang River and other rivers in the surrounding area. Both quality and quantity of the river water should be important as the freshwater influence to the marine environment.

Influence of Water Mixing on Phytoplankton Pigment Composition in Ariake Sound

It is known that phytoplankton can produce photoprotective and light-harvesting pigments under strong and weak light, respectively. However, light environment of phytoplankton in the field varies with vertical water movement. When the mixed layer is shallower as compared to the euphotic zone, the average light received by surface phytoplankton is high. Under these conditions, phytoplanktons produce photoprotective pigments and not light-harvesting pigments. In Ariake Sound, the sediment resuspended by strong tidal mixing causes shallow euphotic zone. Under this condition, it is expected that the response of phytoplankton under large light variation is easily observed. Thus, a difference in phytoplankton pigments was observed during the spring and the neap tides in winter with euphotic zone and light diffuse attenuation coefficient.

The observation was conducted by T/V Kakuyo-Maru of Nagasaki University on December 11–12 (spring tide) and December 17–18 (neap tide), 2008. Vertical density distributions were observed by a thermo-salinometer and the depth of the mixed layer (Z_{mix}) was estimated. The light attenuation coefficient (k_d) was estimated from the vertical distribution of photosynthetically active radiation. The average relative radiation ($\overline{I_{\mathrm{mix}}}$) was calculated using the following equation;

$$\overline{I_{\mathrm{mix}}} = 100 \times \frac{1 - \mathrm{e}^{k \times Z_{mix}}}{k \times \mathrm{Z}_{mix}}.$$

Chlorophyll-a, which is the basic pigment for photosynthesis is known to increase under low light conditions, light-harvesting accessory pigments (fucoxanthin and peridin), and photo-protected pigments (diadinoxanthin and diatoxanthin) were measured by high-performance liquid chromatography.

The mixed layer was deeper and the light attenuation coefficient was larger during the spring tide as compared with the neap tide (Fig. 5). This may be due to strong tidal currents made the deeper mixed layers and more resuspension of the bottom sediments during the spring tides. Thus, from the spring to the neap tides, the mixed layer became shallower, the attenuation coefficient decreased, and the average light intensity increased.

On the other hand, the chlorophyll-a concentration was low in the spring tide and increased in the neap tide. The fraction of light-harvesting accessory pigments (fucoxanthin and peridinin) per chlorophyll-a was nearly constant, although that of photo-protective pigments per chlorophyll-a increased from the spring to the neap tides.

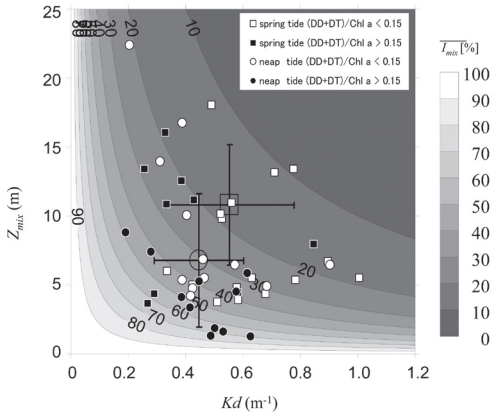

Fig. 5. Scatter plot of mixed layer depth (Z_{mix}) versus light attenuation coefficient (K_d) for samples obtained during spring (square) and neap (circle) tides. Contour lines show averaged relative light intensity in the euphotic zone ($\overline{I_{\mathrm{mix}}}$). Crosses indicate the means and standard deviations of the squares and circles. Open and closed symbols indicate the ratio of (diadinoxanthin + diatoxanthin)/Chlorophyll-a [(DD + DT)/Chl-a] < 0.15 and > 0.15, respectively. Mean value of (DD + DT)/Chlorophyll-a is 0.15.

These results indicate that a decrease in the mixed layer and attenuation coefficient caused increase of the average light intensity for phytoplankton from the neap to the spring tide, and that phytoplankton responded to increase photo-protective pigments per chlorophyll-a to acclimatize to the strong light environment.

Seasonal Variations in Primary Productivity, Particle Flux, and Air-Sea CO_2 Flux in the Sagami Bay

A part of the particles produced in the upper ocean by phytoplankton is vertically carried to the deep layer. This process plays a major role in CO_2 sequestration to the deep ocean and is known as the biological pump. To examine the factors controlling the variability in the strength of the biological pump in Sagami Bay, we have analyzed the quantity and quality of the sinking particles collected by a moored sediment trap (at a depth of 150 m). These samples were collected over a period of one week, beginning in January 2001. Here we report the results of the data collected from November 2007 to December 2008, when the POPPS (Project on Ocean Productivity Profiling System) buoy system provides productivity data from the same region, and discuss seasonal variations in primary productivity and particle flux.

The net primary productivity (NPP) was low in winter (200–400 mg C m^{-2} d^{-1}), and increased from spring to a maximal value during August/September (>1200 mg C m^{-2} d^{-1}) (Fig. 6). Following this, the particulate organic carbon flux at a depth of 150 m (POC $flux_{150\ m}$) exhibited an increase from spring to summer, with a maximum during September/October (>70 mg C m^{-2} d^{-1}), which lagged the peak of NPP by about a month (Fig. 6).

The $\delta^{15}N$ signal of trapped particles marked a minimum (~1.4 permil) in late February and gradually increased to a maximum (9.8 permil) in May (Fig. 6), suggesting that nutrients supplied due to winter mixing were gradually consumed by phytoplankton during spring. In early June, $\delta^{15}N$ showed a steep decline (~7 permil) and remained stable at these levels. This implies that seasonal fresh-water discharge and/or episodic, cyclonic eddies deliver nutrient-rich waters into the euphotic zone (EZ), which would sustain higher NPP and POC $flux_{150\ m}$ during summer.

During the entire period, the averaged NPP and POC $flux_{150\ m}$ were 579.2 mg C m^{-2} d^{-1} and 40.0 mg C m^{-2} d^{-1}, respectively. Another observations using short-term (2–4 days) multi-layer sediment traps showed a sharp drop-off of POC flux with depth at shallower levels. This demonstrated a vertical flux ratio (POC $flux_{150\ m}$/POC $flux_{50\ m}$) of 0.28. With this value, an annual averaged POC $flux_{50\ m}$ of 142.9 mg C m^{-2} d^{-1} and an export ratio at 50 m (=POC $flux_{50\ m}$/NPP) of 0.25 were estimated. Given a mean EZ of 50 m in the Sagami Bay, this export ratio would correspond to the *f*-ratio. That is, in terms of nitrogen, 25% of the annual production is fueled by nitrogenous nutrients supplied from outside the EZ, known as new production.

Since the $\delta^{13}C$ of suspended POC within the EZ of Sagami Bay was strongly correlated with pCO_2 in the surface waters, it is possible to apply this empirical regression to $\delta^{13}C$ of trapped particles (Fig. 6). Then, changes in the surface oceanic pCO_2 were reconstructed and the air-sea CO_2 flux was estimated during the observation period. The averaged CO_2 flux was –72.9 mg C m^{-2} d^{-1}, suggesting that the Sagami Bay acts as a sink for atmospheric CO_2. Higher CO_2 absorption (<–100 mg C m^{-2} d^{-1}) occurred during March/July and October/November (Fig. 6). Using the annual average of the air-sea CO_2 flux, 55% of the CO_2 absorption was explained by POC $flux_{150\ m}$, indicating that more than half of the absorbed CO_2 was transported to the deep sea as sinking POC. This conclusion emphasizes the importance of the biological pump in the absorption of CO_2 in Sagami Bay.

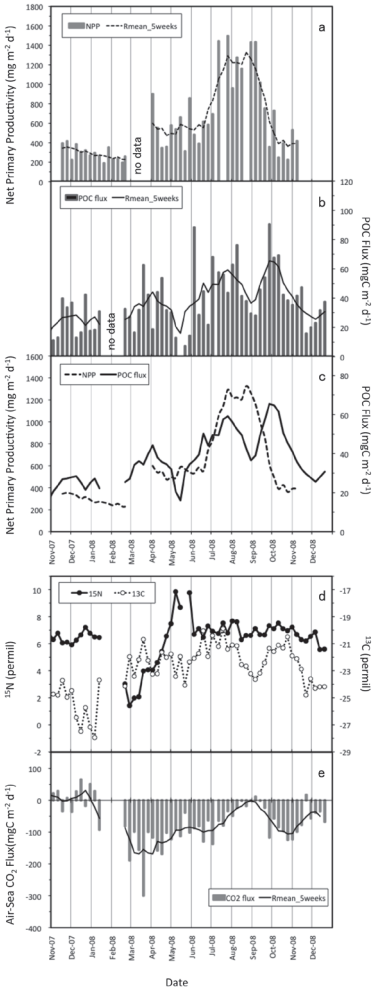

Fig. 6. Temporal changes in (a) NPP, (b) downward POC flux at a depth of 150 m, (c) five-week running mean for NPP (dotted line) and POC flux (solid line), (d) $\delta^{15}N$ and $\delta^{13}C$ of trapped organic matter, and (e) air-sea CO_2 flux in central Sagami Bay.

Laboratory of Bio-Physical Oceanography

Interannual variation in nutrient transport through the Tsushima Strait

The Tsushima Warm Current carries large amounts of freshwater and nutrients from the East China Sea (ECS) to the Japan Sea (JS). The water quality and discharge rates of the Changjiang change rapidly. It is hypothesized that changes in the marine environment of the ECS may influence that in the JS. In order to investigate this, we studied the seasonal and interannual variations in the nutrient transport through the Tsushima Strait (TS). Since long-term nutrient data are limited, we derived empirical equations using in-site dissolved inorganic nitrogen (DIN) and water temperature data from the TS. These equations were formulated using 22 times hydrographic observations from 2005 to 2008. Applying the empirical equations to water temperature data taken in June, August, and October from 1971 to 2000 in the TS, we estimated the DIN concentration and the DIN transports through both the eastern (ECTS) and western (WCTS) channels of the TS. The results indicated that the 30-year averages of DIN transport through the ECTS in June, August, and October were 2.09 kmol/s, 3.55 kmol/s, and 4.10 kmol/s, respectively. The 30-year averages of DIN transport through the WCTS in June, August, and October were 7.40 kmol/s, 9.64 kmol/s, and 13.39 kmol/s, respectively. Interannual variations in the DIN transport through the ECTS and WCTS in August were considerably large (Fig. 1), because there is a large year to year variation in the DIN concentration or water temperature in the lower layer of the TS. Comparing the variations in DIN transport to the salinity distribution in the TS revealed that salinity in the surface layer of the WCTS in June, August, and October and of the ECTS in August tends to be lower when DIN concentrations are higher than average value. This suggests that a relationship between the occurrence of low temperature water in the bottom layer in the TS and the freshwater inflow from the ECS into the surface layer in the TS.

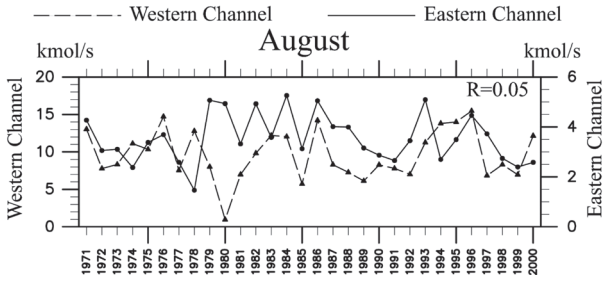

Fig.1. Interannual variation in DIN transport through TS in August from 1971 to 2000. The right and left vertical axes indicate DIN transport through the WCTS and ECTS, respectively.

Improved current velocity calculation algorithm for Long Range Ocean Radar

The National Institute of Information and Communications (NICT) has established the long range ocean radar (LROR) system at Ishigaki and Yonaguni Islands in the Yaeyama archipelago, Japan. Since 2001, high temporal and spatial resolution measurements of sea-surface currents (SSC) around Yaeyama Islands have been conducted using LROR. According to design specifications, the LROR can measure SSC over an area of 200 km from the radar site; however data calculated by the present algorithm covered approximately only 120 km from the radar site. The SSC is calculated from Doppler spectral data (SP data) of the LROR. Analysis of the SP data reveals that SSC data can be obtained in situations where present algorithm shows no data or unrealistic SSC. Using this SP data, we improved current velocity calculation algorithm, and then reprocessed SP data from 2004 to 2007.

To calculate the SSC, the primary peak, which is the frequency with the largest spectral energy, must be determined. Parameters for detecting the primary peak were derived by trial and error using SP data of August 2004. FORTRAN was used to prepare data processing tools. Using this new algorithm, the SP data from 2004 to 2007 were reprocessed and both SSC data sets (those calculated by the previous and newly derived algorithms) were compared. The spatial distribution of the SSC data acquired are similar, but the root mean square (RMS) of

the SSC on the continental shelf processed by the newly developed algorithm is much smaller than that processed by the previous algorithm (Fig. 2). This result suggests improved accuracy of the data acquired father from radar site.

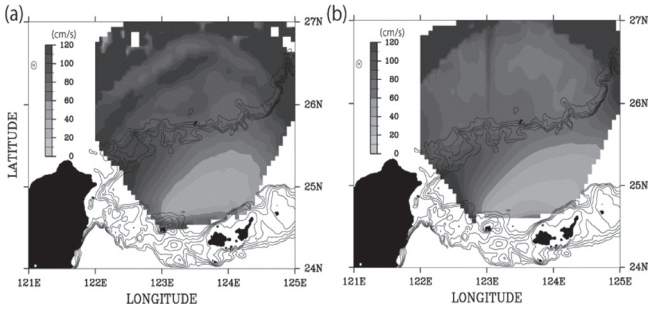

Fig.2. (a) RMS of SSC processed by the previous algorithm, (b) RMS of SSC processed by the present algorithm. The contour lines indicate bottom topography.

Seasonal variation in the Kuroshio northeast of Taiwan

The velocity and axial position of the Kuroshio northeast of Taiwan varies at intervals that can be greater than 30 days. However, there is limited knowledge about the seasonal variation because of description and discussion using short-term and discontinuous data in the previous study. The Kuroshio has been monitored since 2001 to the present day using the LROR provided by the NICT. The LROR has provided surface current data with high spatial and temporal resolution. This study investigates the seasonal variation of the velocity and axial position of the Kuroshio using the LROR surface current data.

The Kuroshio has stable northeastward currents with speeds greater than 50 cm s^{-1} and flow fluctuations with magnitudes of approximately 40 cm s^{-1} along its axis (Fig. 3a). The seasonal variations in the maximum northeastward current and axial position are shown in Fig. 3b (line AB). Here, the maximum northeastward current is defined as the maximum current speed of the northeastward current on line AB. The axial position is defined as the distance from point A to the location of the maximum northeastward current on line AB. The seasonal variation in the maximum northeastward current consists of long- and short-term seasonal variations. The long-term seasonal variation had winter minimum (~65 cm s^{-1} in January), summer maximum (~115 cm s^{-1} in July), and a periodicity of approximately 1 year. The short-term seasonal variation was predominant during April to November and characterized by a maximum in July and minimums in May and October. The Kuroshio axis moved northwestward from its mean position (solid square in Fig. 3b) within a range of about 20 km. The seasonality of the Kuroshio's axis movement was not clear (Fig. 3b). In addition, the long- and short-term seasonal variations were closely related to the seasonal variations of the meridional component of wind stress around the ECS and of the Sverdrup transport over the area from the ECS to north of the Philippine Basin, respectively. This suggests that the seasonal variation in velocity of the Kuroshio occurs in response to wind forcing not over the North Pacific Ocean but over the local areas from the ECS to the north of the Philippine Basin.

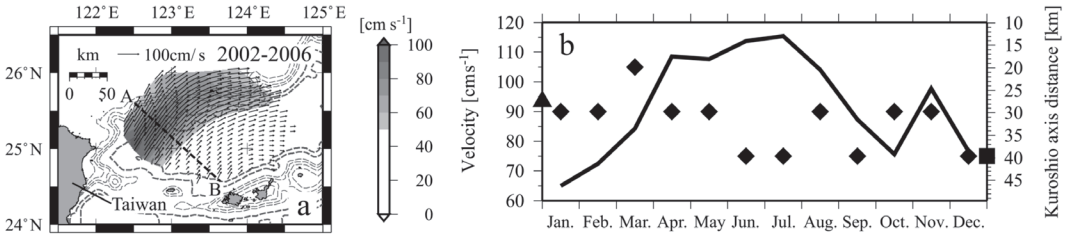

Fig.3. (a) Mean surface current during the period from 2002 to 2006. (b) Seasonal variations in the maximum northeastward current (solid line) and axial position of the Kuroshio (solid diamond) on line AB. The shaded area in (a) represents currents with speeds greater than 50 cm s^{-1}. The solid triangle and square in (b) represent the maximum northeastward current and the axial position of the Kuroshio in the mean surface current field in (a), respectively.

34 List of Publications

* : Staffs, students and research fellows in the HyARC.

1. Abe, O., S. Agata, M. Morimoto, M. Abe, K. Yoshimura, T. Hiyama* and N. Yoshida
   A 6.5-year continuous record of sea surface salinity and seawater isotopic composition at Harbor of Ishigaki island, southwest Japan. *Isotopes in Environmental and Health Studie*s, **45**, 247-258, 2009.
2. Endoh, T., T. Matsuno, Y. Yoshikawa, Y. Tatsuyama and J. Ishizaka*
   Observations of wind-driven deepening of the surface mixing layer in the Tsushima Strait. *Journal of Oceangraphy,* **65**, 273-279, 2009.
3. Friedrichs, M.A.M., M.-E. Carr, R.T. Barber, M. Scardi, D. Antoine, R.A. Armstrong, I. Asanuma, M.J. Behrenfeld, E.T. Buitenhuis, F. Chai, J.R. Christian, A.M. Ciotti, S.C. Doney, M. Dowell, J. Dunne, B. Gentili, W. Gregg, N. Hoepffner, J. Ishizaka*, T. Kameda, I. Lima, J. Marra, F. Melin, J.K. Moore, A. Morel, R.T. O'Malley, J. O'Reilly, V.S. Saba, M. Schmeltz, T.J. Smyth, J. Tjiputra, K. Waters, T.K. Westberry and A. Winguth
   Assessing the uncertainties of model estimates of primary productivity in the tropical Pacific Ocean. *Journal of Marine Systems*, **76**, 113-133, 2009.
4. Fukutomi, Y. and T. Yasunari*
   Cross-equatorial Influences of Submonthly scale Southerly surges over the eastern Indian Ocean during Southern Hemisphere winter. *Journal of Geophysical Research*, **114**, D20119, 15, 2009.
5. Geng, B., H. Yamada, K.K. Reddy, H. Uyeda* and Y. Fujiyoshi
   Mesoscale Development and Along-Frontal Variation of a Meiyu/Baiu Front and Precipitation Observed in the Downstream Region of the Yangtze River. *Journal of the Meteorological Society of Japan*, **87**(3), 423-457, 2009.
6. Fujinami, H.* and T. Yasunari*
   The effects of midlatitude waves over and around the Tibetan Plateau on submonthly variability of the East Asian summer monsoon. *Monthly Weather Review,* **137**, 2286-2304, doi: 10.1175/2009MWR2826.1. 2009.
7. Hirose, M., R. Oki, D.A. Short* and K. Nakamura*
   Regional characteristics of scale-based precipitation systems from 10-year TRMM PR data. *Journal of the Meteorological Society of Japan*, **87A**, 353-368, 2009.
8. Ichikawa, H.*, H. Masunaga* and H. Kanzawa
   Evaluation of Precipitation and High-level Cloud Areas Associated with Large-scale Circulation over the Tropical Pacific in the CMIP3 Models. *Journal of the Meteorological Society of Japan*, **87**(4), 771-789, 2009.
9. Ishida, H., Y.W. Watanabe, J. Ishizaka*, T. Nakano, N. Nagai, Y. Watanabe, A. Shimamoto, N. Maeda and M. Magi
   Possibility of recent changes in vertical distribution and size composition of chlorophyll-a in the western North Pacific region. *Journal Oceanography,* **65**, 179-186, 2009.
10. Ishizaka, J.*
    Ocean Color Research for Global Imager (GLI) on Advanced Earth Observation Satellite-II (ADEOS-II). *Journal of Remote Sensing Society of Japan*, **29**, 74-79, 2009.
11. Jianqing, Xu, S. Yu, J. Liu, S. Haginoya, Y. Ishigooka, T. Kuwagata, M. Hara and T. Yasunari*
    The implication of heat and water balance change in a Lake Basin on the Tibetan Plateau. *Hydrological Research Letters,* 3.1-5. doi: 10.3178/HRL.3.1, 2009.
12. Kim, H.-C., H. Yamaguchi*, S. Yoo, J. Zhu, K. Okamura, Y. Kiyomoto, K. Tanaka, S.-W. Kim, T. Park, I.S. Oh and J. Ishizaka*
    Distribution of Changjiang Diluted Water detected by satellite chlorophyll-a and its interannual variation during 1998–2007. *Journal of Oceanography*, **65**, 129-135, 2009.
13. Liu, P., M. Satoh, B. Wang, H. Fudeyasu, T. Nasuno, T. Li, H. Miura, H. Taniguchi, H. Masunaga*, X. Fu and H. Annamalai
    An MJO simulated by the NICAM at 14-km and 7-km resolutions. *Monthly Weather Review*, **137**,

3254-3268, 2009.

14. Liu, P., Y. Kajikawa*, B. Wang, A. Kitoh, T. Yasunari*, T. Li, H. Annamalai, X. Fu, K. Kikuchi, R. Mizuta, K. Rajendran, D.E. Waliser and D. Kim
Tropical Intraseasonal Variability in the MRI-20km 60L AGCM. *Journal of Climate*, **22**, 2006-2022, 2009.
15. Masunaga, H.*
A 9-season TRMM observation of the Austral Summer MJO and Low-frequency Equatorial Waves. *Journal of Meteorological Society of Japan*, **87A**, 295-315, 2009.
16. Matsui, T., X. Zeng, W.-K. Tao, H. Masunaga*, W.S. Olson and S. Lang
Evaluation of Long-term Cloud-resolving Model Simulations Using Satellite Radiance Observations and Multi-frequency Satellite Simulators. *Journal Atmospheric and Oceanic Technology*, **26**, 1261-1274, 2009.
17. Morimoto, A.*
Evaluation of Tidal Error in Altimetry Data in the Asian Marginal Seas. *Journal of Oceanography*, **65**(4), 477-485, 2009.
18. Morimoto, A.*, S. Kojima, S. Jan and D. Takahashi*
Movement of the Kuroshio axis to the northeast shelf of Taiwan during typhoon events. *Estuarine, Coastal and Shelf Science*, **82**(3), 547-552, 2009.
19. Morimoto, A.*, T. Takikawa, G. Onitsuka, A. Watanabe, M. Moku and T. Yanagi
Seasonal Variation of Horizontal Material Transport through the Eastern Channel of the Tsushima Straits. *Journal of Oceanography*, **65**(1), 61-71, 2009.
20. Morimoto, A.*, Y. Isoda, T. Tameishi and S. Moriwaki
Seasonal variation in Tsushima Warm Current paths over the shelf off the San'in coast, Japan. *Continental Shelf Research*, **29**(11-12), 1437-1447, 2009.
21. Nakajima, T., H. Murakami, M. Hori, T.Y. Nakajima, H. Yamamoto, J. Ishizaka*, R. Takeishi, T. Aoki, T. Takamura, M. Kuji, D.D. Nguyen, A. Ono, S. Fukuda and K. Muramatsu
Overview and Science Highlights of the ADEOS-II/GLI Project. *The Remote Sensing Society of Japan*, **29**, 11-28, 2009.
22. Nakajima, T.Y., H. Masunaga* and T. Nakajima
Near-global Scale Retrievals of the Cloud Optical and Microphysical Properties from the Midori-II GLI and AMSR Data. *The Remote Sensing Society of Japan*, **29**, 29-39, 2009.
23. Nishikawa, M.*, T. Hiyama*, K. Tsuboki* and Y. Fukushima
Numerical Simulations of Local Circulation and Cumulus Generation over the Loess Plateau, China. *Journal of Applied Meteorology and Climatology*, **48**, 849-862, 2009.
24. Ohigashi, T*. and G.W.K. Moore
Fine structure of a Greenland reverse tip jet: A numerical simulation. *Tellus*, **61A,** 512- 526, 2009.
25. Onitsuka, G., A. Morimoto*, T. Takikawa, A. Watanabe, M. Moku, Y. Yoshikawa and T. Yanagi
Enhanced chlorophyll associated with island-induced cyclonic eddies in the eastern channel of the Tsushima Straits. *Estuarine, Coastal and Shelf Science*, **81**(3), 401-408, 2009.
26. Oouchi, K.A., T. Noda, M. Satoh, B. Wang, S.P. Xie, H.G. Takahashi and T. Yasunari*
Asian summer monsoon simulated by a global cloud-system-resolving model: diurnal Intra-seasonal Variability. *Geophysical Research Letters,* **36**. L11815. doi: 10.1029/ 2009GL038271. 2009.
27. Padhakrishna, B., T. Narayana Rao, D. Narayana Rao, N. Prabhakara Rao, K. Nakamura* and Ashok Kumar
SharmaSpatial and seasonal variability of raindrop size distributions in southesast India. *Journal of Geophysical Research*, **114**, D04203, doi: 10.1029/2008JD011226, 2009.
28. Rao, D.N., M.V. Ratnam, S. Mehta, D. Nath, S. Ghouse Basha, V.V.M. Jagannadha Rao, B.V. Krishna Murthy, T. Tsuda and K. Nakamura*
Validation of the COSMIC radio occultation data over Gadangi (13.48N, 79.2E): A tropical region. *Terrestrial Atmospheric and Oceanic Science*. **20**(1), 59-70, doi: 10: 3319/TAO2008.01.23.01(F3C), 2009.
29. Shinoda, T.*, A. Higuchi, K. Tsuboki*, T. Hiyama*, H. Tanaka*, S. Endo*, H. Minda*, H. Uyeda* and K. Nakamura*

Structure of convective circulation in the atmospheric boundary layer over the northwestern Pacific Ocean under a subtropical high. *Journal of the Meteorological Society of Japan*, **87**(6), 979-996, 2009.

30. Shinoda, T.*, T. Amano, H. Uyeda*, K. Tsuboki* and H. Minda*
Structure of line-shaped convective systems obliquely training to the Baiu front observed around the Southwest Islands of Japan. *Journal of the Meteorological Society of Japan*, **87**(4), 739-745, 2009.
31. Short, D.A.*, M. Hirose and K. Nakmaura*
An interpretation of TRMM radar observations of shallow convection with a rain cell model. *Journal of the Meteorological Society of Japan*, **87A**, 53-66, 2009.
32. Shusse, Y.*, K. Nakagawa, N. Takahashi, S. Satoh and T. Iguchi
Characteristics of polarimetric radar variables in three types of rainfalls in a Baiu front event over the East China Sea. *Journal of the Meteorological Society of Japan*, **87**(5), 865-875, 2009.
33. Singh, P.* and K. Nakamura*
Diurnal variation in summer precipitation over the central Tibetan Plateau. *Journal of Geophysical Research*, **114**, D20107, doi: 10.1029/2009JD011788, 2009.
34. Siswanto, E.*, A. Morimoto* and S. Kojima
Enhancement of phytoplankton primary productivity in the southern East China Sea following episodic typhoon passage. *Geophysical Research Letters*, **36**, L11603, 2009.
35. Takahashi, D.*, X. Guo, A. Morimoto* and S. Kojima
Biweekly periodic variation of the Kuroshio axis northeast of Taiwan as revealed by ocean high-frequency radar. *Continental Shelf Research*, **29**(15), 1896-1907, 2009.
36. Takata, K., K. Saito and T. Yasunari*
Changes in the Asian monsoon climate during 1700–1850 induced by pre-industrial cultivation. Proceedings of the National Academy of Sciences of the United States of Ameirica, doi: 10.1073/pnas.0807346106, 2009.
37. Prasanna, V. and T. Yasunari*
Time-space characteristics of seasonal and intrannual variations of atmospheric water balance over south Asia. *Journal of the Meteorological Society of Japan*, **87**(2), 263-287. 2009.
38. You, C.-H., D.-I. Lee, S.-M. Jang, H. Uyeda*, T. Shinoda* and F. Kobayashi
Characteristics of Rainfall Systems Accompanied with Changma Front at Chufado in Korea. *Asia-Pacific Journal of Atmospheric Sciences*, **46**(1), 41-51, 2009.
39. Morimoto, A.*
Horizontal and Vertical Nutrients transport in the Eastern Channel of the Tsushima Strait, Monitoring and prediction of marine and atmospheric environmental change in the East Asia, Ed. T. Yanagi, TERAPUB, 171-194, 2010.

Hydrospheric Atmospheric Research Center (HyARC)

Nagoya University

Furo-cho, Chikusa-ku, Nagoya 464-8601, Japan

Office:

Telephone: +81-52-789-3466

Facsimile: +81-52-789-3436

Home Page: http://www.hyarc.nagoya-u.ac.jp/english/index.html

The 2009 Annual Report was published October 2010 by the Hydrospheric Atmospheric Research Center (HyARC) Nagoya University. Copies of this report are available from the office of the Center.

Printed by Nagoya University COOP


HyARC
Hydrospheric Atmospheric Research Center, Nagoya University